ACS OMEGA

http://pubs.acs.org/journal/acsodf

Article

Design, Synthesis, Computational Investigations, and Antitumor Evaluation of *N*-Rhodanine Glycosides Derivatives as Potent DNA Intercalation and Topo II Inhibition against Cancer Cells

Ahmed I. Khodair,* Fatimah M. Alzahrani, Mohamed K. Awad, Siham A. Al-Issa, Ghaferah H. Al-Hazmi, and Mohamed S. Nafie

Cite This: *ACS Omega* 2023, 8, 13300−13314

Read Online

ACCESS | Metrics & More | Article Recommendations | Supporting Information

ABSTRACT: Nitrogen and sulfur glycosylation was carried out via the reaction of rhodanine (**1**) with α-acetobromoglucose **3** under basic conditions. Deacetylation of the protected nitrogen nucleoside **4** was performed with CH_3ONa in CH_3OH without cleavage of the rhodanine ring to afford the deprotected nitrogen nucleoside **6**. Further, deacetylation of the protected sulfur nucleoside **5** was performed with CH_3ONa in CH_3OH with the cleavage of the rhodanine ring to give the hydrolysis product **7**. The protected nitrogen nucleosides **11a−f** were produced by condensing the protected nitrogen nucleoside **4** with the aromatic aldehydes **10a−f** in C_2H_5OH while using morpholine as a secondary amine catalyst. Deacetylation of the protected nitrogen nucleosides **11a−f** was performed with $NaOCH_3/CH_3OH$ without cleavage of the rhodanine ring to afford the deprotected nitrogen nucleosides **12a−f**. NMR spectroscopy was used to designate the anomers' configurations. To examine the electrical and geometric properties derived from the stable structure of the examined compounds, molecular modeling and DFT calculations using the B3LYP/6-31+G (d,p) level were carried out. The quantum chemical descriptors and experimental findings showed a strong connection. The IC_{50} values for most compounds were very encouraging when evaluated against MCF-7, HepG2, and A549 cancer cells. Interestingly, IC_{50} values for **11a**, **12b**, and **12f** were much lower than those for Doxorubicin (7.67, 8.28, 6.62 μM): (3.7, 8.2, 9.8 μM), (3.1, 13.7, 21.8 μM), and (7.17, 2.2, 4.5 μM), respectively. Against Topo II inhibition and DNA intercalation, when compared to Dox (IC_{50} = 9.65 and 31.27 μM), compound **12f** showed IC_{50} values of 7.3 and 18.2 μM, respectively. In addition, compound **12f** induced a 65.6-fold increase in the rate of apoptotic cell death in HepG2 cells, with the cell cycle being arrested in the G2/M phase as a result. Additionally, it upregulated the apoptosis-mediated genes of P53, Bax, and caspase-3,8,9 by 9.53, 8.9, 4.16, 1.13, and 8.4-fold change, while it downregulated the Bcl-2 expression by 0.13-fold. Therefore, glucosylated Rhodanines may be useful as potential therapeutic candidates against cancer because of their topoisomerase II and DNA intercalation activity.

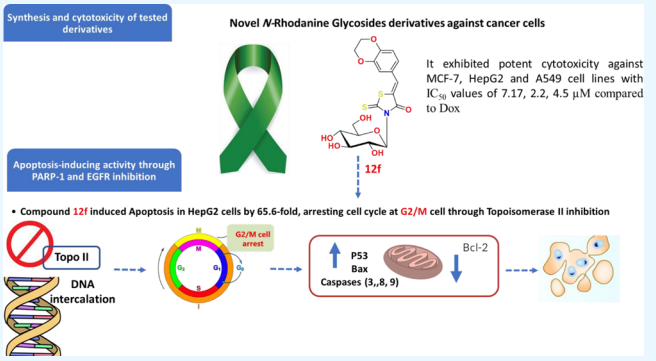

1. INTRODUCTION

Heterocyclic compounds are extensively used by medicinal chemists in their hunt for novel bioactive molecules. Most significantly, the presence of nitrogen-containing heterocycles in a wide range of naturally occurring and synthetically manufactured compounds with well-established biological activity suggests that these heterocycles themselves have a broad range of biological activities. Rhodanine rings have typically been the favored framework for the synthesis of molecules having therapeutic potential. Rhodanine is a heterocyclic compound having the following molecular formula: C2 = thiocarbonyl, N3 = nitrogen, and C4 = carbonyl. The diverse array of useful biological features displayed by rhodanine compounds, including antibacterial activity,[1] antifungal activity,[2] anti-inflammatory activities,[3] antituberculosis,[4] anti-HIV,[5] antiparasitic activity,[6] hypnotic activity,[7] and antihelminthic activity[8] has piqued the curiosity of medicinal chemists. Research on the potential of certain heterocyclic small molecules as effective anticancer drugs has been conducted extensively in recent years. Rhodanine-based derivatives[9−18] exhibited remarkable biological properties as anticonvulsant, antibacterial, antiviral, Hepatitis C Virus (HCV), and antidiabetic medicines, making them a privileged scaffold in the field of drug development.[19−26] As potential

Received: January 31, 2023
Accepted: March 16, 2023
Published: March 28, 2023

tumor aggregation inhibitors, radonine and other 2-thioxo-4-thiazolidinone alternatives have recently been investigated.[27−29] Rhodanine and its bioisostere 2,4-thiazolidinedione (TZD) are examples of heterocyclic substances with a thiazolidine nucleus.[30,31] Figure 1 shows that rhodanine

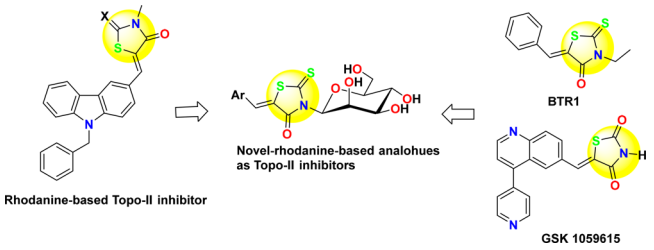

Figure 1. Pharmacophore hybridization strategy for designing novel potential rhodinine derivatives with Topo-II inhibition activity.

derivatives can be promising scaffold with Topo-II inhibition activity.[32] One of these mimics (ERK) is Raf/MEK/extracellular signal-regulated kinase, and pathways for Wnt signal transduction have been connected to carcinogenesis, tumor development, and metastasis.[33] A novel, ATP-competitive, and reversible PI3Ka inhibitor is GSK1059615.[34] This potential therapeutic candidate has a thiazolidinone ring connected to a pyridinylquinoline via an ethene segment. 5-Benzylidene-3-ethyl rhodanine (BTR-1) was described to exhibit broad anticancer activity with IC_{50} lower than 10 μM, using the same justification. Rhodanine in BTR-1 is part of an arylidine system.[32] Despite these activities, research into anticancer drugs from this class that have less side effects while still being effective is still in its infancy. Previous investigations of structurally similar heterocyclic system glycosyl derivatives were published.[35−46]

Computational chemistry has been developed over the past few decades with linking architecture and functions of organic and biological processes. In order to understand structures, molecular characteristics, processes, and reaction selectivity, computations have become crucial.[47−53] One of the most widely used theoretical techniques for calculating a wide range of molecular properties is the density functional theory (DFT).[18,54,55] Thermodynamic properties, molecular structures, vibrational frequencies, chemical shifts, nonlinear optical NLO effects, natural bond orbital NBO analyses, electrostatic molecular potential, and density of molecular orbitals are all estimated using this method. We keep working on the synthesis of novel nucleosides as possible antiviral and anticancer drugs in light of the biological significance of rhodanines.[40,43,56,57] Here, we describe the synthesis of several *N*-glucosylated bases containing rhodamine, as well as their anticancer screening and spectroscopic analysis. Also, we examined the effects of modifications to the compounds under investigation's molecular and electrical structure on their biological activity using the density functional theory. The objective of the ROCS analysis was to identify the key features of our compounds and to explain their 3D-QSAR.

These adjustments represented in Figure 1 were made to improve the design strategy. To enhance the drug's pharmacokinetics, a sugar moiety was inserted between the rhodanine ring and the arylidine ring, and the arylidine ring was replaced with a substituted arylidine ring (similar to BTR-1).

We looked at further synthetic methods for producing rhodanine nucleosides for use as antiviral and anticancer medications as part of our ongoing study in this area. In this investigation, we present the synthesis, conformational characterization, and anticancer screening of a number of nitrogen glycosylated compounds.

Scheme 1. Synthesis of 2-thiothiazolidin-4-one derivatives 4−6

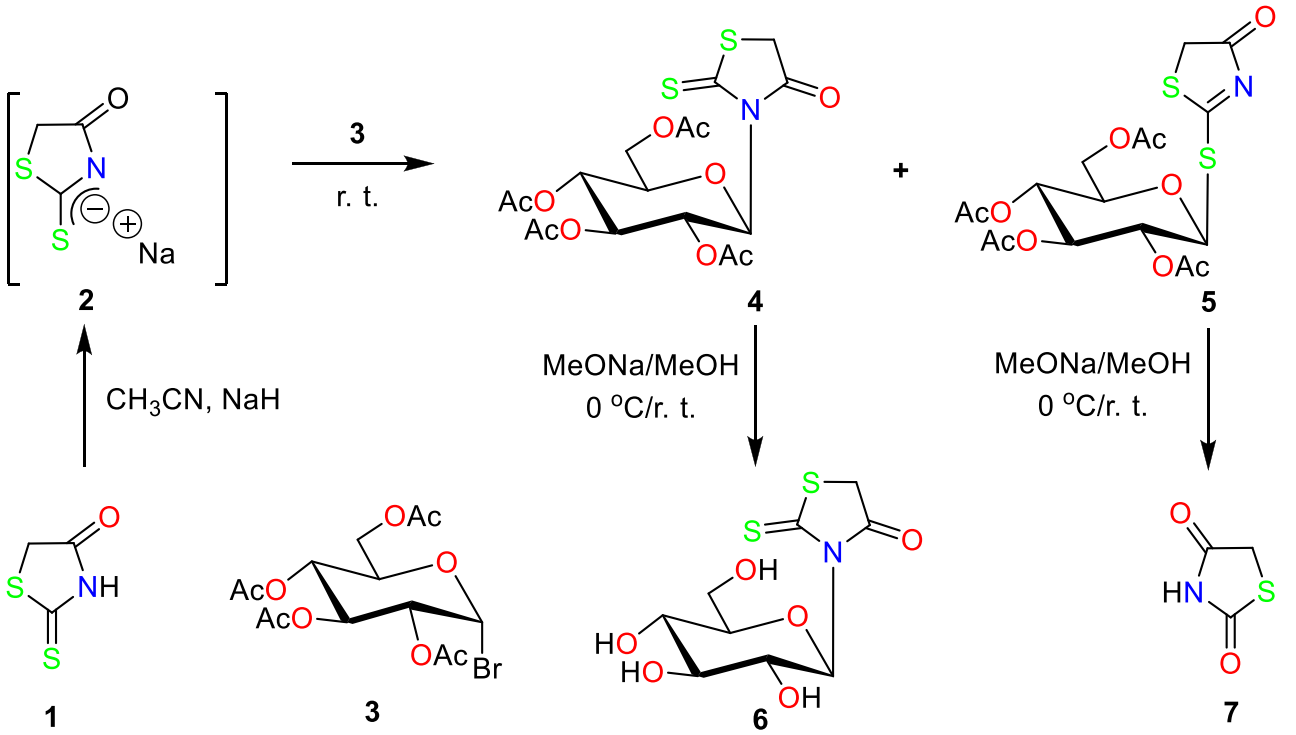

https://doi.org/10.1021/acsomega.3c00641
ACS Omega 2023, 8, 13300−13314

2. RESULTS AND DISCUSSION

2.1. Chemistry. The sodium salt of rhodanine (**2**) was produced by reacting nucleoside base **1** with 1.1 equiv of NaH in anhydrous acetonitrile, which in turn was reacted with 1.1 equiv of 2,3,4,6-tetra-*O*-acetyl-α-D-glucopyranosyl bromide (**3**) to afford 3-(2′,3′,4′,6′-tetra-*O*-acetyl-β-D-glucopyranosyl)-2-thioxo-4-thiazolidinone (**4**) (69%) and 2-(2′,3′,4′,6′-tetra-*O*-acetyl-β-D-glucopyranosylmercapto)-4-thiazolidinone (**5**) (4%) compared to the prior silylation technique using bis-(trimethylsilyl)acetamide (BSA), which produced yields of 6% of **4** and 30% of **5** for the same nucleoside base **1**.[58] By using elemental analysis and spectrum data, the structures of **4** and **5** were constructed and verified (IR, ^{1}H NMR, ^{13}C NMR, and MS). IR absorption spectra of compound **4** were distinguished by the absence of an NH signal and the presence of a thiocarbonyl group signal at ν_{max} 1225 cm^{-1}. The IR absorption spectrum of chemical **5** was distinctive, but there was no sign of a thiocarbonyl group. The anomeric proton of compound **4** appearing as a doublet in the ^{1}H NMR spectrum at δ_H 6.82 ppm (J = 9.30 Hz) revealed the existence of the α-D-glucopyranose moiety.[36−40] In the ^{13}C NMR spectra of compound **4**, the carbonyl group at C-4 and the thiocarbonyl group at C-2 are each characterized as singlets (300 MHz, $CDCl_3$). These results concur with the ^{13}C NMR spectrum of 3-(piperidin-1-ylmethyl)-2-thioxothiazolidin-4-one (**8**) ($CDCl_3$) at 300 MHz (Scheme 2). The latter was produced by reacting **1** with piperidine and formaldehyde in EtOH at room temperature since the carbonyl at C-4 appears at δ_C 175.1 ppm and the thiocarbonyl group at C-2 appears at δ_C 203.2 ppm, suggesting that *N*-glycosylation is present. The presence of the β-D-glucopyranose moiety was demonstrated by the anomeric proton, which showed up as a doublet at δ_H 5.82 ppm (J = 10.4 Hz) in the ^{1}H NMR spectra of compound **5**.[35−39] The carbonyl at C-4 and the thiocarbonyl group at C-2 in compound **5** both had a singlet in the spectrum of the ^{13}C NMR (300 MHz, $CDCl_3$). Additionally, these results are consistent with the ^{13}C NMR (300 MHz, $CDCl_3$) spectrum of the previously identified 2-methylmercapto-4-thiazolidinone (**9**).[58] While the C-2 thiocarbonyl group appears at δ_C 202.5 ppm in Scheme 2, where the C-2 methylmercapto appears at δ_C 15.9 ppm, the C-4 carbonyl appears at δ_C 187.1 ppm, showing the presence of *S*-glycosylation. Indicating *N*-glycosylation, the protected nucleoside **4** was treated with $NaOCH_3$/MeOH at room temperature to produce the corresponding deprotected nucleotide **6**. Similarly, treatment of **5** with $NaOCH_3$/MeOH at room temperature produced the previously recognized 2,4-thazolidinedione (**7**)[59] suggesting *S*-glycosylation. Our attempts to create the corresponding deprotected nucleoside of **5** failed due to this form of cleavage (Scheme 1).

Scheme 2. Synthesis of 3-(piperidin-1-ylmethyl)-2-thiothiazolidin-4-one (8) and 2-methylmercaptothiazolidin-4-one (9)

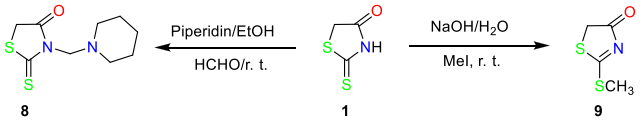

The required aromatic aldehydes (**10a−f**) were condensed with the protected nucleoside **4** in ethanol with morpholine serving as a catalyst to create the requisite 5-((*Z*)-arylidene-3-(2′,3′,4′,6′-tetra-*O*-acetyl-β-D-glucopyranosyl)-2-thioxo-4-thiazolidinones (**11a−f**). 5-((*Z*)-Arylidene)-3-(β-D-glucopyranosyl)-2-thioxo-4-thiazolidinones were produced by treating the glycon moieties of **11a−f** with a sodium methoxide solution in methanol to remove the acetyl groups (**12a−f**). The condensation of **6** with benzaldehyde (**10a**) in EtOH with morpholine as a catalyst occurred at room temperature, and this process was used to independently synthesize the deprotected nucleoside **12a**. The structures of **11a−f** and **12a−f** were established and confirmed using elemental studies and spectrum data (IR, ^{1}H NMR, ^{13}C NMR, and MS). The carbonyl and thiocarbonyl groups as well as the absence of a signal for NH were present in the IR absorption spectra of compound **11a**. ^{1}H NMR (300 MHz, $CDCl_3$) spectrum of compound **11a** revealed a vinyl proton singlet at δ_H 7.73 ppm, indicating the exocyclic double bond has a *Z*-configuration. This is consistent with the ^{1}H NMR spectra of 5-((*Z*)-benzylidene)-3-methyl-2-thio-4-thiazolidinone, which has a vinyl proton at H 7.75 ppm (300 MHz, $CDCl_3$)[60] and 5-

Scheme 3. Synthesis of 5-((*Z*)-arylidene-3-(2′,3′,4′,6′-tetra-*O*-acetyl-β-D-glucopyranosyl)-2-thioxo-4-thiazolidinones (11a−f) and 5-((*Z*)-arylidene-3-(β-D-glucopyranosyl)-2-thioxo-4-thiazolidinones (12a−f)

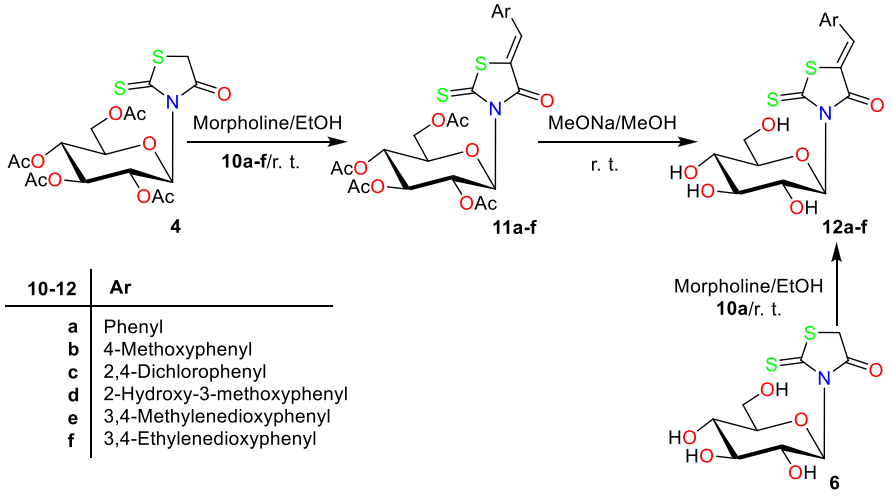

10-12	Ar
a	Phenyl
b	4-Methoxyphenyl
c	2,4-Dichlorophenyl
d	2-Hydroxy-3-methoxyphenyl
e	3,4-Methylenedioxyphenyl
f	3,4-Ethylenedioxyphenyl

https://doi.org/10.1021/acsomega.3c00641
ACS Omega 2023, 8, 13300−13314

((*Z*)-benzylidene)-3-(2′,3′,4′,6′-tetra-*O*-acetyl-*β*-D-mannopyranosyl)-2-thioxo-4-thiazolidinone whose vinyl proton appears at δ_H 7.69 ppm,[18] while the coupling constant $J_{1'-2'}$ for the diaxil interaction is 9.40 Hz for the anomeric proton 1′-H of the glucopyranosyl moiety, which provides a doublet at δ_H 6.35 ppm. A *β*-glucopyranosyl anomer is characterized by this high coupling constant.[35−39] The spectrum of compound **11a** obtained by ^{13}C NMR (300 MHz, $CDCl_3$) showed a singlet at δ_C 165.9 and 194.1 ppm, which was attributable to the carbonyl group at C-4 and the thiocarbonyl group at C-2, respectively. These observations are also supported by the ^{13}C NMR ($CDCl_3$) spectra of 5-((*Z*)-hexylidene-4-oxo-2-thioxothiazolidinyl)-acetic acid.[56] Also, these findings are consistent with the 5-((*Z*)-hexylidene-4-oxo-2-thioxothiazolidinyl)-acetic acid ^{13}C NMR ($CDCl_3$) spectrum,[61] where the presence of *N*-glycosylation is shown by the carbonyl group at C-4 appearing at δ_C 165.7 ppm and the thiocarbonyl group at C-2 appearing at δ_C 194.8 ppm (Scheme 3).

3. MOLECULAR MODELING DETAILS

The molecular structures of the substances under examination were optimized using density functional theory (DFT), and Beck's three parameter exchange functional, the Lee−Yang−Parr nonlocal correlation functional (B3LYP), as well as the basis set 6-31+G(d,p), are both implemented in the software program Gaussian 09.[62−64] The DFT/B3LYP combination was used to calculate an estimate of the molecular characteristics associated with molecular reactivity. The following relationships affected the molecular properties, such as the occupied highest molecular orbital (HOMO), the unoccupied lowest molecular orbital (LUMO), hardness, electronegativity, ionization potential, and electron affinity:

$$I = -E_{HOMO} \qquad A = -E_{LUMO} \qquad \mu = -\chi$$

$$\mu = \frac{(E_{HOMO} + E_{LUMO})}{2}$$

$$\eta = \frac{(E_{LUMO} + E_{HOMO})}{2}$$

The softness is the opposite of hardness, σ: $\sigma = 1/\eta$.

3.1. Quantum Chemical Details. Many molecular parameters contribute to the description of reactivity; shape and binding properties of whole molecules, molecular fragments, and substituents can all be specified using quantum chemistry techniques and molecular modeling tools. The impact of structural factors on the biological activity of several researched substances was examined using quantum chemical calculations. The computations proved that the researched organic molecules' geometrical structures are not planned. In order to start our computations, we compared the stability of the compounds under investigation in both their *Z*- and *E*-forms. The computations showed that the investigated compounds are 0.009 to 0.051 au more stable in the *Z*-form than the *E*-form for all the molecules we examined, which is in good accord with the experimental data. Thus, we performed DFT calculations on the stable Z-form structures of each molecule.

3.2. Compound 11a vs 12a. Figure 2 displays the calculated molecular structures of the substances studied, which are optimized for minimal energy. The calculations were done to investigate the effect of replacing the 2-acetoxy methyl groups, **11a**, by 2-hydroxymethyl groups, **12a**, on the biological activity of the 5-benzylidene-2-thioxothiazoline-4-one compound. In summary, the presence of 2-hydroxymethyl groups was proven to improve the reactivity of the inhibitor, **12a**, with respect to the **11a** molecule using the quantum chemical parameters acquired from the calculations.

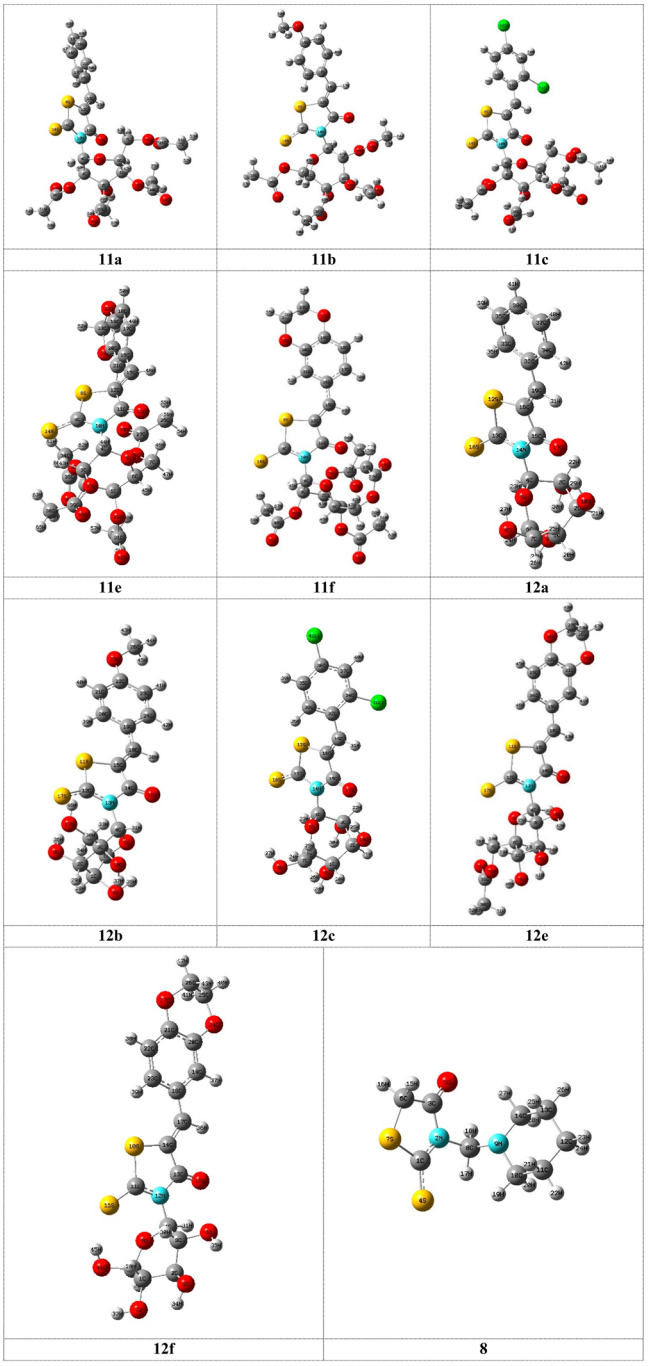

Figure 2. Computationally optimized molecular structures of the inhibitors under study.

According to the frontier molecular orbital (FMO) theory, chemical reactivity is determined by the interplay between the HOMO and LUMO levels of the interacting species. The electron-donating ability of a molecule is represented by the E_{HOMO} symbol, and the electron-accepting ability is represented by the E_{LUMO} symbol. E_{LUMO} is proportional to the molecule's receptivity to accepting electrons. Increases in E_{HOMO} value for an inhibitor correlate with enhanced

https://doi.org/10.1021/acsomega.3c00641
ACS Omega 2023, 8, 13300−13314

Table 1. Quantum Chemical Parameters of the Studied Compounds as Determined Using DFT/B3LYP/6-31+G(d)

Compound	HOMO (au)	LUMO (au)	ΔE (au)	Dipole (D)	IP (au)	EA (au)	η (au)	σ (au^{-1})	μ (au)	χ (au)	E_t (au)
11a	−0.243	−0.111	0.132	6.561	0.243	0.111	0.066	15.152	−0.177	0.177	−2519.564
11b	−0.227	−0.103	0.124	11.522	0.227	0.103	0.062	16.129	−0.165	0.165	−2633.447
11c	−0.252	−0.124	0.128	4.372	0.252	0.124	0.064	15.625	−0.188	0.188	−3434.345
11e	−0.223	−0.100	0.123	10.464	0.223	0.100	0.062	16.129	−0.162	0.162	−2707.003
11f	−0.227	−0.105	0.122	12.869	0.227	0.105	0.061	16.393	−0.166	0.166	−2746.138
12a	−0.237	−0.109	0.128	2.886	0.237	0.109	0.064	15.625	−0.173	0.173	−1912.264
12b	−0.215	−0.095	0.120	11.142	0.215	0.095	0.060	16.666	−0.155	0.155	−2026.143
12c	−0.241	−0.123	0.118	0.835	0.241	0.123	0.059	16.949	−0.182	0.182	−2827.046
12e	−0.214	−0.087	0.127	6.127	0.214	0.087	0.064	15.625	−0.151	0.151	−2138.854
12f	−0.222	−0.097	0.125	6.209	0.222	0.097	0.063	15.873	−0.159	0.159	−2099.756
8	−0.212	−0.062	0.150	2.740	0.212	0.062	0.075	13.333	−0.137	0.137	−1325.641

inhibition because the inhibitor is better able to supply electrons to the metal surface's unoccupied d-orbital.

When comparing the reactivity between compounds **11a** and **12a**, the insertion of the hydroxymethyl substituent increases the energy of the HOMO of **12a** inhibitor by 0.006 au, which indicates that this substance has a higher degree of reactivity than **11a** (Table 1), since it has the potential to behave as an electron donor in chemical reactions. In addition, the HOMO−LUMO energy gap, ΔE, is used to create theoretical models that explain the structure and conformational barriers of many different molecular systems. The smaller the value of ΔE is, the more probable it is that the compound has inhibition efficiency. The calculations showed that inhibitor **12a** has a smaller ΔE (0.128 au) than that of **11a** inhibitor (0.132 au), which is most likely accountable for increasing the biological activity for **12a** compound compared to inhibitor **11a**, Table 1. The structure was discussed and justified with reference to the dipole moment, D, the first derivative of the energy with respect to an applied electric field. D correlates positively with inhibitory effectiveness. This was shown from the decrease of the dipole moment of compound **12a** (2.886 D) with respect to that of compound **11a** (6.563 D), Table 1. The absolute hardness and softness of a molecule are useful quantities for gauging its stability and reactivity. An energetic gap is larger for hard molecules and narrower for soft ones. Since soft molecules may readily donate electrons to an acceptor, they are considered to be more reactive than their rigid counterparts. In a biological system, the inhibitor acts as a Lewis base, while the enzyme as a Lewis acid, . Compared to **11a**, whose softness and electronegativity are both 15.152 au^{-1} and 0.177 au, **12a** inhibitor's softness and electronegativity are both 15.625 au^{-1} and 0.173 au, respectively, which may explain the organism's enhanced biological activity, Table 1.

Accordingly, we could expect from the above results obtained from the calculations that **12a** inhibitor has a higher reactivity than **11a** which means that it could be more biologically active.

3.3. Compounds 11b,c vs 12b,c. Experimentally, it was found that the insertion of methoxy- and dichloro- groups on the 5-(cyclohexa-1,5-dien-1-ylmethylene)-2-thiooxothiazolidine-4-one moiety decreases the biological activity in the case of 2-(acetoxymethyl)-6-(5-benzylidene)-4-oxo-2-thioxothiazloidin-3-yl) tetrahydro-2*H*-pyran-3,4,5-triacetate, inhibitors **11b,c**, while it increases in the case of 5-(benzylidene)-2-thioxo-3,4,5-(trihydroxymethyl)tetrahydro-2*H*-pyran-2-yl)-thiazolidine-4-one, inhibitors **12b,c**. This was confirmed from reducing HOMO energy for compounds **11b,c** (−0.227 and −0.252 au) while increasing the HOMO energy for inhibitors **12b** and **12c** (−0.215 and −0.241 au) , Table 1, which means increasing the ability of **12b,c** compounds to act as nucleophiles on interaction with enzyme and accordingly increases their reactivity compared with that of compounds **11b,c**. This is in good agreement with the experimental observations. Also, the energy gap, ΔE, between HOMO−LUMO could be responsible for decreasing the reactivity for compounds **11b,c**, with respect to **12b,c** compounds. Higher ΔE values for compounds **11b,c** (0.124 and 0.128 au) were shown compared to those for **12b,c** compounds (0.120 and 0.118 au) , which agrees well with experimental observations.

Meanwhile, decreasing the softness of compounds **11b,c** (16.129 and 15.625 au^{-1}) could increase their stabilities and accordingly decrease the biological activity compared to increasing the reactivity for compounds **12b,c** due to an increase in the softness (16.666 and 16.949 au^{-1}). In addition, decreasing the reactivity for compounds **11b,c** could be due to increasing their electronegativity (0.165 and 0.188 au), more than those of compounds **12b,c** (0.155 and 0.182 au), Table 1.

We could conclude from the preceding discussion that the reactivity of 5-(benzylidene)-2-thioxo-3,4,5-(trihydroxymethyl)tetrahydro-2*H*-pyran-2-yl)thiazolidine-4-one, with methoxy and dichloro groups, **12b,c**, is higher than that of 2-(acetoxymethyl)-6-(5-benzylidene)-4-oxo-2-thioxothiazloidin-3-yl)tetrahydro-2*H*-pyran-3,4,5-triacetate compounds, **11b,c**, which agrees well with the experimental findings.

Comparing the effects of substituents in the same nucleus, 2-(acetoxymethyl)-6-(5-benzylidene)-4-oxo-2-thioxothiazloidin-3-yl) tetrahydro-2*H*-pyran-3,4,5-triacetate, inhibitor **11a**, on the biological activity was also studied using DFT calculations. It could be seen experimentally that the presence of the methoxy group, compound **11b**, increased the biological activity more than that of dichloro- groups, compound **11c**. This could probably be due to decreasing the chemical potential, IP, the energy gap, ΔE, and the electronegativity, χ, and increasing the softness, σ, and dipole moment, Table 1. By contrast, the dichloro- group in the case 5-(benzylidene)-2-thioxo-3,4,5-(trihydroxymethyl)tetrahydro-2*H*-pyran-2-yl)-thiazolidine-4-one, **12a**, possibly contributing to an increase the reactivity with relation to the effect of the methoxy group. This was shown from the decreasing the energy difference between HOMO−LUMO, ΔE, dipole moment, D, and increasing the energy of LUMO, softness, and electronegativity, Table 1, which is in good agreement with experimental observation.

3.4. Compounds 11e,f vs 12e,f. In contrast to the above results, the substituted 2-(acetoxymethyl)-6-(5-benzylidene)-4-

https://doi.org/10.1021/acsomega.3c00641
ACS Omega 2023, 8, 13300−13314

oxo-2-thioxothiazloidin-3-yl)tetrahydro-2*H*-pyran-3,4,5-triacetate with 1,3-dioxolane and 1,4-dioxane, **11e** and **11f**, respectively, showed higher biological activity than the substituted 5-(benzylidene)-2-thioxo-3,4,5-(trihydroxymethyl)tetrahydro-2*H*-pyran-2-yl)thiazolidine-4-one, **12e** and **12f**. This could be due to decreasing energy of LUMO for **11e,f** (−0.100 and −0.105 au) more than that of **12e,f** (−0.087 and −0.097 au). This means that compounds **11e,f** have a greater tendency to accept electrons from enzymes than **12e,f** which leads to an increase in their reactivity compared to **12e,f** inhibitors. Also, the more reactive compounds, **11e,f**, have lower ΔE values (0.123 and 0.122 au) than those of **12e,f** inhibitors (0.127 and 0.125 au). Meanwhile, increasing the dipole moment (10.464, 12.869 D), softness (16.129 and 16.393 au^{-1}) and chemical potentials (−0.162 and −0.166 au) for inhibitors **11e,f**, Table 1, could be responsible for increasing their reactivities which is in a good agreement with experimental observations.

We could conclude from the above discussion that the reactivity of 2-(acetoxymethyl)-6-(5-benzylidene)-4-oxo-2-thioxothiazloidin-3-yl)tetrahydro-2*H*-pyran-3,4,5-triacetate with 1,3-dioxolane and 1,4-dioxane substituents, **11e,f** is higher than that of compounds 5-(benzylidene)-2-thioxo-3,4,5-(trihydroxymethyl)tetrahydro-2*H*-pyran-2-yl)thiazolidine-4-one, **12e,f**, which is congruent with the experimental data.

To compare the effects of 1,4-dioxolane and 1,4-dioxane substituents on the reactivity of inhibitors **11e,f** and **12e,f**, we observed that the 1,4-dioxane substituent increased the reactivity of inhibitors **11f** and **12f** more than that of 1,3-dioxolane in inhibitors **11e** and **12e**. This could be shown from the decreasing energy of LUMO, ΔE, and increasing dipole moment, softness, and chemical potential for inhibitors **11f** and **12f** over those of **11e** and **12e**, Table 1, which agrees well with experimental results.

3.5. Frontier Molecular Orbitals FMO. The way a molecule interacts with other molecules is influenced by the widely used quantum chemistry characteristics known as the HOMO and LUMO levels. Figures 2 and 3 display the charge density distribution at the HOMO and LUMO levels for the compounds under investigation. The investigated compounds, **11a−f**, demonstrated that the HOMO levels, which could react with the biological target as a nucleophile "hydrogen bond acceptor", are just primarily localized on the lone-pairs of sulfur, nitrogen, and oxygen atoms of the thioxothiazolidine moiety and with charge density as C−C character on the benzylidene moiety, with the exception of compounds **11b** and **11c** with methoxy and dichoro substituents with localization on thioxothiazolidine moiety only. All compounds under investigation have sugar moieties, yet they have no effect on the HOMO level. The benzylidene-2-thioxothiazolidine moiety with π^* character is where the majority of the LUMO level is located, which can react with the biological target as an electrophile "hydrogen bond donor". Figure 3 shows that the sugar moiety has no effect on the HOMO and LUMO levels. Calculations revealed that charge transfer from nucleophilic sites to electrophilic regions of the same molecules is possible. However, it was discovered that the HOMO level in compound **12a** is primarily restricted to the sugar moiety. By contrast, for compounds **12b−f**, it is primarily focused on the entire molecule, with the exception of the sugar moiety, and is contributed by lone pairs of S, N, and O atoms as well as a charge density of π C−C character. Delocalization

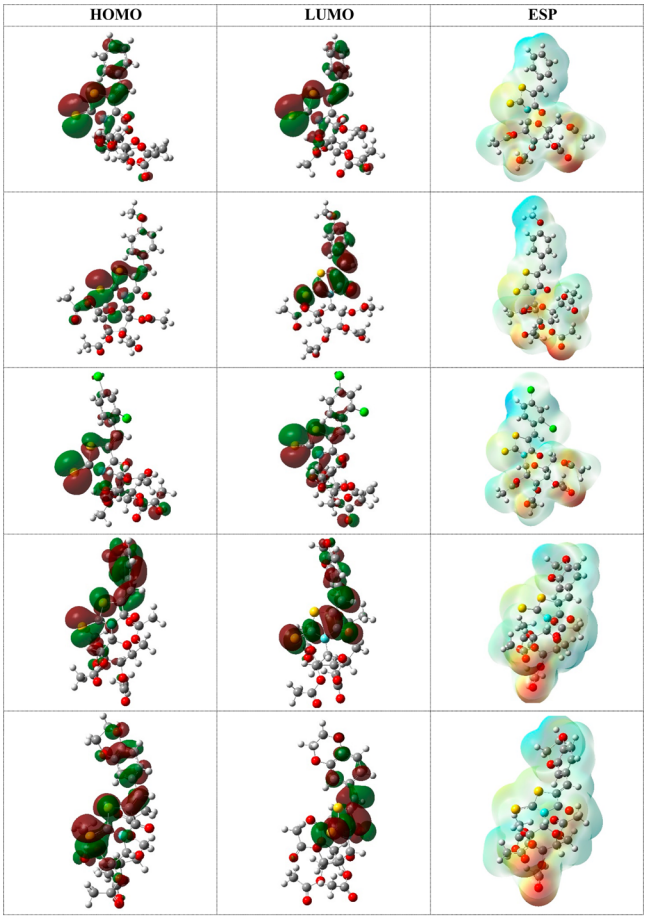

Figure 3. Charge distribution for the HOMO, LUMO, and MEP for compounds **11a−f**.

of the LUMO level occurs over the whole molecule except for sugar moiety for **12b−f**, Figure 4.

As a result of FMOs, it was determined that the effect of substituents on the benzylidene moiety is crucial for increasing the affinities of the tested compounds for the target enzymes.

3.6. Molecular Electrostatic Potential (MEP−MAPS). The molecular electrostatic potential (MEP), at which it is connected to the electronic thickness, is one of the most significant and helpful descriptors that are used to understand the regions for electrophilic assault and nucleophilic reactions. The B3LYP method and the basis set of 6-31G (d,p) were used to compute the molecular electrostatic potentials in optimal geometry in order to estimate the enzyme's reactive areas for electrophilic and nucleophilic assaults. Different colors, such as red, orange, yellow, green, and blue, show different levels of the electrostatic potential on the surface. The possible increases are indicated by the colors red, orange, yellow, green, and blue. As shown in Figures 3 and 4, positive regions (blue) are related with nucleophilic reactivity, while negative areas (red and yellow) are associated with electrophilic reactivity.

The electrophilic reactivity sites are represented by red color regions of MEP, and the nucleophilic reactivity ones are represented by blue color. The negative charge (electrophilic attack sites) covers the thioxothiazolidine moiety of the investigated compounds, while the positive regions are above the benzylidine moiety. The MEP plots can shed light on the

https://doi.org/10.1021/acsomega.3c00641
ACS Omega 2023, 8, 13300−13314

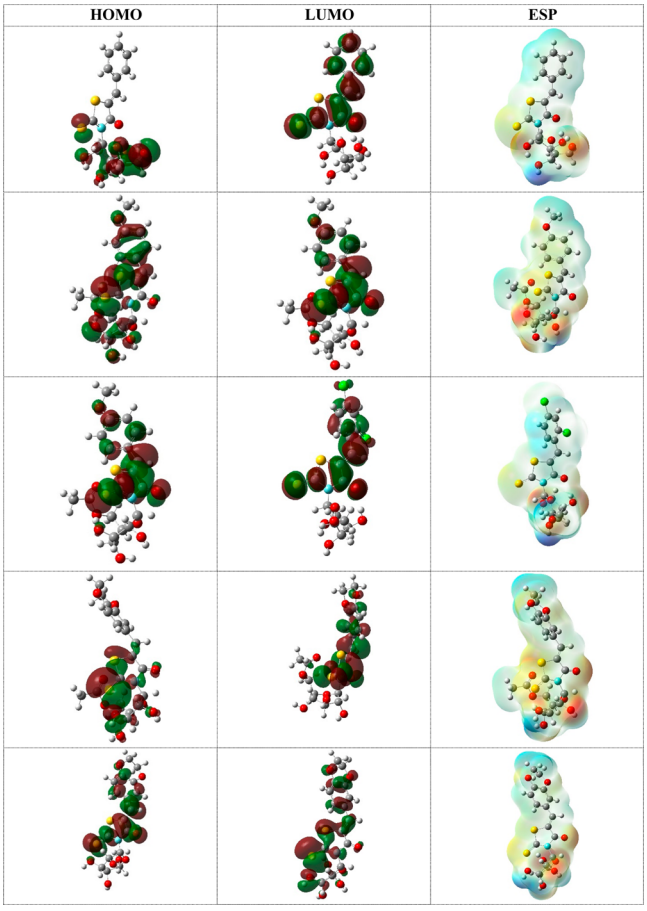

Figure 4. Charge distribution for the HOMO, LUMO, and MEP for compounds **12a−f**.

electrostatic interaction forces between the probed molecules and the biological target.

3.7. Compound 8: 3-(piperidin-1-ylmethyl)-2-thioxothiazolidin-4-one. Molecular modeling calculations were done to see the correlation between quantum chemical parameters and biological activity of 3-(piperidin-1-ylmethyl)-2-thioxothiazolidin-4-one, inhibitor **8**. The optimized molecular structure with minimum energy obtained from the calculations of the investigated compound **8** is shown in Figure 2. Experimental results and computed quantum characteristics both showed that inhibitor **8**, 3-(piperidin-1-ylmethyl)-2-thioxothiazolidin-4-one, was biologically inactive. The calculations showed that compound **8** has a low HOMO (−0.212 au) and a high LUMO (0.062 au), which increase the difference between HOMO−LUMO to be the highest energy gap, ΔE (0.150 au), among the other investigated inhibitors, Figure 5. This means increases its stability and accordingly becomes biologically inactive, which is consistent with experimental findings, Table 1. There is a good correlation between dipole moment and inhibition efficiency. The lower the dipole moment, the higher the stability of the molecule, and accordingly it is biologically inactive. This was shown from decreasing the dipole moment of compound **8** (2.740 D). Absolute hardness, η, and softness, σ, are functions of the stability of a molecule. Since soft molecules may readily donate electrons to an acceptor, they are more reactive than their rigid counterparts. In a biological system, the inhibitor acts as a Lewis base while the enzyme as a Lewis acid. The decreasing

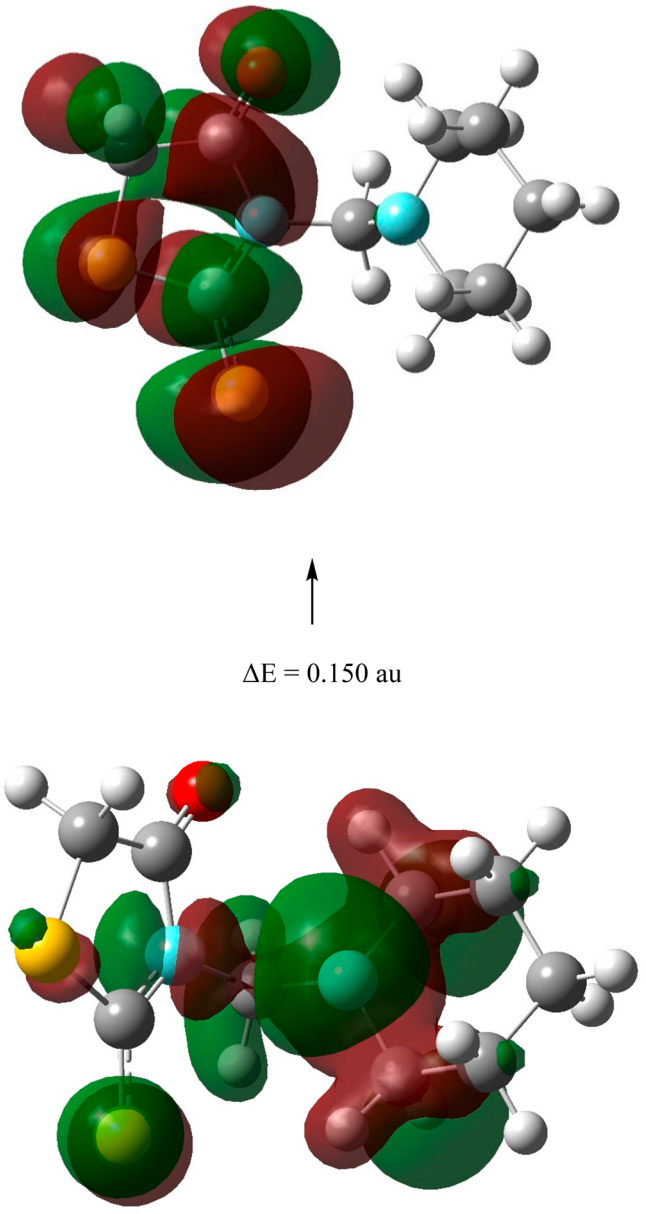

Figure 5. Optimized molecular structures and charge density distributions (HOMO and LUMO) for the compound **8**.

the softness and chemical potential of inhibitor **8** (13.333 au^{-1}, and −0.137 au) could be responsible for decreasing its biological activity, Table 1, which agrees well with the experimental observations.

The MTT assay was used to test the synthetic compounds for cytotoxicity against breast, liver, and lung cancer cells. IC_{50} values for cytotoxicity against MCF-7, hepG2, and A549 cells are shown in Table 2, indicating that most of these compounds are promising. Interestingly, compared to Dox (7.67, 8.28, 6.62 μM), compounds **11a**, **12b**, and **12f** displayed significant cytotoxicity with IC_{50} values of (3.7, 8.2, 9.8 μM), (3.1, 13.7, 21.8 μM), and (7.17, 2.2, 4.5 μM), respectively. The compounds with IC_{50} values above 50 were found to be inactive. Accordingly, the molecular target and apoptotic activity of compounds **11a**, **12b**, and **12f** were studied.

Investigating the cytotoxicity of the most cytotoxic compound **12f** against normal breast MCF-10A, liver THLE2, and lung WISH cells. As seen in Figure 6, compound

https://doi.org/10.1021/acsomega.3c00641
ACS Omega 2023, 8, 13300−13314

Table 2. IC_{50} values of the tested compounds against MCF-7, HepG2, and A549 cell lines using the MTT assay[a]

Code	IC_{50} (μM ± SD[a])		
	MCF-7	HepG2	A549
8	ND	45.9 ± 1.32	ND
11a	3.7 ± 0.13	8.2 ± 0.14	9.8 ± 0.11
11b	11.7 ± 0.24	12.2 ± 0.46	18.7 ± 1.04
11c	16.7 ± 0.33	4.7 ± 0.11	ND
11e	7.2 ± 0.14	ND	10.1 ± 0.21
11f	6.1 ± 0.16	11.3 ± 0.37	17.1 ± 0.43
12b	3.1 ± 0.11	13.7 ± 0.39	21.8 ± 0.62
12c	13.7 ± 0.15	12.1 ± 0.16	11.3 ± 0.42
12e	21.1 ± 0.56	23.7 ± 0.36	ND
12f	7.17 ± 0.16	2.2 ± 0.11	4.5 ± 0.16
Doxorubicin	7.67 ± 0.12	8.28 ± 0.45	6.62 ± 0.24

[a]Values are expressed as Mean ± SD of three independent values. ND = Not Determined.

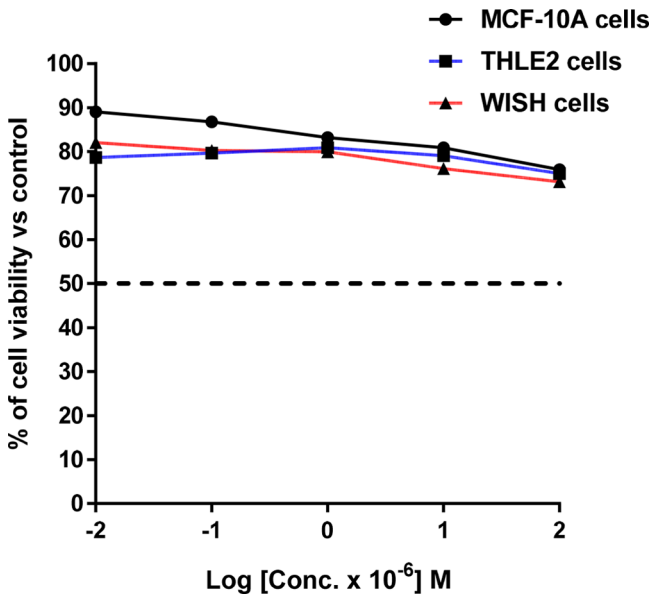

Figure 6. Percentage of cell viability compared to control versus concentration [0.01−100 μM] using the MTT assay. The IC_{50} values for the cytotoxicity of compound **12f** against normal cells were not determined.

12f exhibited low cytotoxicity having cell viability of nearly 75% at the highest concentration [100 μM]. Hence, this compound was noncytotoxic against the normal cells.

4. TOPO II AND DNA INTERCALATION ASSAY

Mechanistic studies were highlighted by testing the Topo II and DNA intercalation activities of the most cytotoxic compounds against HepG2 cells, **11a**, **12b**, and **12f**. Interestingly, compared to Dox (IC_{50} = 9.65 and 31.27 μM), compound **12f** demonstrated IC_{50} values of 7.3 and 18.2 μM for dual Topo II and DNA intercalation activities, respectively (Table 3). The IC_{50} values for compounds **11a** and **12b** were 7.6 and 9.2 μM for Topo II and 31.6 and 32.4 μM for DNA intercalation, respectively, demonstrating promising inhibitory activity. As a result, the possibility of apoptotic cell death in HepG2 cells was further explored using compound **12f**.

4.1. Apoptotic Investigation 12f against HepG2 Cells. The apoptotic activity of compound **12f** (IC_{50} = 0.22 μM, 48 h) was determined by analyzing apoptotic cell death in untreated and treated HepG2 cells using flow cytometric evaluation of Annexin V/PI staining. Figure 7A indicated that compound **12f** increased apoptotic cell death in HepG2 cells by 65.6-fold. It caused total apoptosis by 44.65% (29.13% for early apoptosis, 15.52% for late apoptosis) compared to the untreated control group (0.68%). Following cytotoxic treatment, DNA flow cytometry was used to quantify the percentage of cells in each phase of the cell cycle. As seen in Figure 7B, the percentage of cells in the G2/M-phase was 34.51% higher in the compound **12f** group than in the control group, which was 22.13%; there was no obvious increase in G1-phase cells and a decrease in S-phase cells. Therefore, **12f** caused apoptosis in HepG2 cells, stopping their growth at the G2/M-phase checkpoint.

Table 3. Compound IC_{50} Values for DNA Intercalation and Topo II Inhibition

Compound	IC_{50} [μM] ± SD[a]	
	Topoisomerase	DNA intercalation DNA/methyl green
11a	7.6 ± 0.24	31.6 ± 0.96
12b	9.2 ± 0.14	32.4 ± 1.01
12f	7.3 ± 0.13	18.2 ± 0.31
Doxorubicin	9.65 ± 0.19	31.27 ± 1.02

[a]Values are expressed as average of three independent replicates. IC_{50} values were calculated using sigmoidal nonlinear regression curve fit of percentage inhibition against five concentrations of each compound.

4.2. RT-PCR of Apoptosis-Inducing Agents 12f Against HepG2 Cells. Gene expression levels of P53, Bax, caspase-3,8,9, and Bcl-2, which mediate apoptosis, were examined using RT-PCR in both untreated and treated HepG2 cells to verify the apoptotic cell death observed after treatment with compound **12f**. As seen in Table 4, compound **12f** induced a 9.53-, 8.9-, 4.16-, 1.13-, and 8.4-fold change in P53, Bax, caspase-3,8,9 proapoptotic genes while inhibiting Bcl-2 expression by 0.13-fold. Thus, these results suggested that compound **12f** treatment induced cell death mostly via the intrinsic pathway, rather than the extrinsic one, and that this was the cause of the observed apoptosis.

4.3. Molecular Docking. As inhibitors of topoisomerase II enzymes are commonly used as effective anticancer medications, a molecular docking research study was conducted to shed insight on the mechanism of binding of the promising chemical **12f** against these enzymes. As can be seen in Figure 8, compound **12f** binds to the proteins active amino acids, Asp 479, Arg 820, Lys 456, and Ser 480, and interacts with the ligand receptor. Docking analysis showed that compound **12f** produced strong binding affinity with a binding energy of −12.57 kcal/mol; it formed three H-bonds with Asp 479 as key amino acids through the −OH group with bond lengths of 1.61, 2.71, and 1.3 Å.

5. CONCLUSION

We successfully completed the synthesis of 3-(2′,3′,4′,6′-tetra-*O*-acetyl-β-D-glucopyranosyl)-2-thioxo-4-thiazolidinone (**4**), 2-(2′,3′,4′,6′-tetra-*O*-acetyl-β-D-glucopyranosyl)-2-thioxo-4-thiazolidinone (**5**), 3-(β-D-glucopyranosyl)-2-thioxo-4-thiazolidinones (**6**), and their corresponding 5-(*Z*)-arylidene derivatives (**11a−f** and **12a−f**). NMR spectroscopy was used to determine

https://doi.org/10.1021/acsomega.3c00641
ACS Omega 2023, 8, 13300−13314

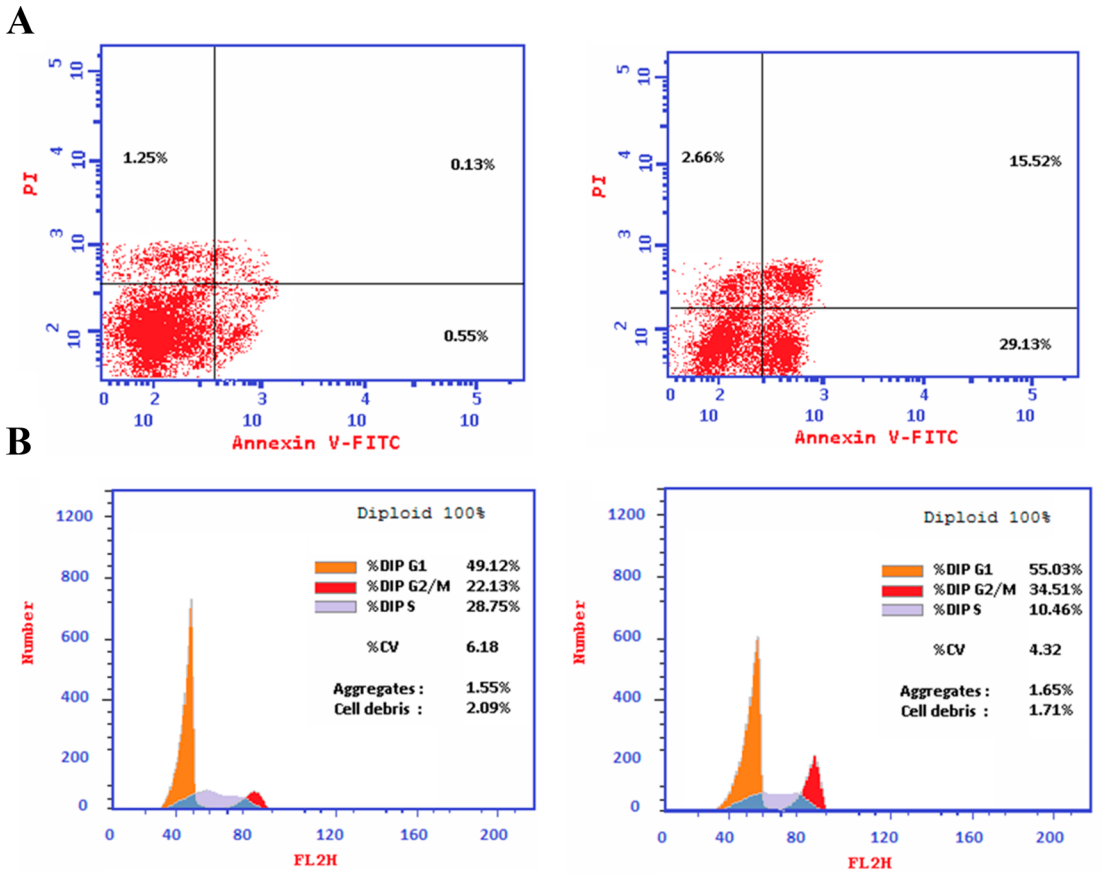

Figure 7. A. Cryptographs of annexin-V/propidium iodide staining of untreated and **12f**-treated HepG2 cells with the IC_{50} values, 48 h, Q1-UL (necrosis, AV-/PI+), Q1-UR (late apoptotic cells, AV+/PI+), Q1-LL (normal cells, AV-/PI-), and Q1-LR (early apoptotic cells, AV+/PI-). **B**. Percentage of cell population at each cell cycle G0-G1, S, G2/M, and Pre-G1 using DNA content-flow cytometry aided cell cycle analysis.

Table 4. Relative Expression of Genes Involved in Apoptosis in Untreated and Treated HepG2 Cells[a]

	Fold Change = $2^{-\Delta\Delta CT}$					
	Pro-apoptotic gene					Anti-apoptotic gene
Sample	P53	Bax	Casp-3	Casp-8	Casp-9	Bcl-2
12f-treated HCT-116	9.53 ± 0.98	8.94 ± 0.87	4.16 ± 0.7	1.13 ± 0.21	8.4 ± 0.7	0.13 ± 0.01
Untreated HepG2	1					

[a]Values are expressed as Mean ± SD of three independent replicates. Data were normalized using β-actin as housekeeping gene.

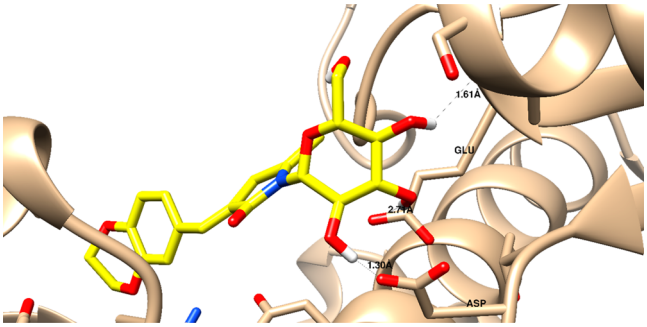

Figure 8. Binding disposition and interactive mode of the docked compound **12f** inside the topoisomeasre II (PDB = 3QX3).

the structural assessments of their most stable configurations. The electrical, geometric, and stable structures of the compounds were investigated using DFT simulations at the B3LYP/6-31+G (d,p) level. The calculated quantum chemical parameters and the experimental findings were well correlated.

Intriguingly, compounds **12f** showed promising cytotoxicity against MCF-7, HepG2, and A549 cells, with IC_{50} values of 7.17, 2.2, and 4.5 μM, respectively, compared to Dox 7.67, 8.28, and 6.62 μM. When compared to Dox, compounds **12f** showed topoisomerase II inhibition and DNA intercalation, with IC_{50} values of 7.3 and 18.2 μM, respectively. Moreover, treatment with compound **12f** greatly increased the rate of apoptosis in HepG2 cells by 65.6-fold, halting the cell cycle during the G2/M phase. As a result, topoisomerase II and DNA intercalation in glucosylated rhodanines may serve as attractive therapeutic candidates for the treatment of cancer.

6. EXPERIMENTAL SECTION

6.1. Chemistry. Melting points were established using a Büchi apparatus and are uncorrected. Short UV light was used to detect TLC on an aluminum sheet coated with silica gel 60 F254 (Merck). Using a Pye Unicam spectrometer 1000, IR spectra were collected for potassium bromide pellets. Using TMS as an internal standard, the ^{1}H NMR and ^{13}C NMR

https://doi.org/10.1021/acsomega.3c00641
ACS Omega 2023, 8, 13300−13314

spectra were measured on Bruker Advance DPX 300 MHz spectrometers in DMSO-d_6 or $CDCl_3$. Chemical shifts are reported in ppm, while J values are given in Hz. A Carlo Erba 1106 C,H,N Elemental Analyzer was used to collect analytical data. EI used a Varian MAT 112 spectrometer to record the mass spectra, while FAB used a Kratos MS spectrometer.

*General Procedures for the Synthesizing **4** and **5**.* At room temperature, rhodanine (**1**) (665 mg, 5 mmol) was dissolved in anhydrous MeCN (5 mL). The mixture was stirred for 30 min at room temperature after NaH was added (50%, 0.26 g, 5 mmol) to this suspension. After 15 min, when the mixture was clear, 2,3,4,6-tetra-*O*-acetyl-α-D-glucopyranosyl bromide (**3**) (2.26 g, 5.50 mmol) was added. The mixture was then stirred for 12 h at room temperature until the starting material was consumed (TLC). The reaction mixture was diluted with 200 mL of CH_2Cl_2, washed with 200 mL of cold, saturated, aqueous $NaHCO_3$, and then dried over anhydrous Na_2SO_4. The mixture was concentrated under vacuum, and the residue was removed using flash chromatography (eluent: 10−50% ether/petroleum ether, 40−60 0C), yielding **4** and **5**. The structural attribution of these compounds **4** and **5** was fully supported by physical and spectral data (Supporting Information).

*General Procedures for the Synthesis of 3-(Piperidin-1-ylmethyl)-2-thioxothiazolidin-4-one (**8**).* Anhydrous ethanol (5 mL), piperidine (85 mg, 1 mmol), aqueous formaldehyde (0.1 mL), and rhodanine (**1**) (665 mg, 5 mmol) were mixed and stirred for 12 h at room temperature until the starting material was consumed (TLC). Filtration was used to collect the separated solid, and it was then recrystallized from the ethanol to produce 184 mg (80%) of **8** as a yellow solid; mp 248−250 °C; IR, KBr (cm^{-1}): 1734 (CO), 1230 (CS); ^{1}H NMR (300 MHz, $CDCl_3$, δ, ppm): 1.32 (1H, q, J = 4.8 Hz, 4′-H), 1.45 (4H, q, J = 4.7 Hz, 3′-H, 5′-H), 2.45 (4H, t, J = 4.7 Hz, 2′-H, 6′-H), 4.25 (2H, s, 5-H), 4.38 (2H, s, NCH_2N); ^{13}C NMR (300 MHz, $CDCl_3$, δ, ppm): 23.92, 25.70, 37.28, 51.44, 65.26, 174.12, 201.98; EI ms: m/z = 230 (M^+); anal. calcd. for $C_8H_{12}N_2O_2S_2$ (230.34): C = 46.93; H, 6.13, N = 12.16; found: C = 46.98, H = 5.82, N = 12.03.

*General Procedures for the Synthesis of **11a−f**.* The protected nucleoside **6** (463 mg, 1 mmol) was combined with the appropriate aromatic aldehydes **10a−f**, anhydrous morpholine (0.09 g, 1 mmol), and anhydrous EtOH (10 mL). After 12 h of stirring at room temperature, the mixture was neutralized with HCl/MeOH. The mixture was filtered after five minutes of stirring. The filtrate was evaporated under vacuum, and the remaining material was then cleaned using flash chromatography (eluent 10−50%, ether/petroleum ether, 40−60 °C), yielding the products **11a−f** as yellow solids.

*5-((Z)-Benzylidene)-3-(2′,3′,4′,6′-tetra-O-acetyl-β-D-glucopyranosyl)-2-thioxo-4-thiazolidinone (**11a**).* This compound has mp 194−196 °C; yield 0.50 (92%) (lit.,[65] mp 192−194 °C, yield 79%); IR, KBr (cm^{-1}): 1750 (C), 1746 (CO), 1225 (CS); ^{1}H NMR (300 MHz, $CDCl_3$, δ, ppm): 1.94, 2.04, 2.07, 2.11 (12H, 4s, 4Ac), 3.87−3.92 (1H, m, 5′-H), 4.22−4.90 (2H, m, 6′-H, 6″-H), 5.29 (1H, dd, J = 9.8, 9.8 Hz, 4′-H), 5.40 (1H, dd, J = 9.4, 9.4 Hz, 2′-H), 6.14 (1H, dd, J = 9.2, 9.2 Hz, 3′-H), 6.35 (1H, d, J = 9.4 Hz, 1′-H), 7.48 (5H, m, 5H, Ar−H), 7.73 (1H, s, =CH); ^{13}C NMR (300 MHz, $CDCl_3$, δ, ppm): 20.40, 20.60, 20.64, 20.78, 61.68, 67.76, 67.81, 73.26, 74.87, 81.80, 120.48, 125.89, 129.35, 129.37, 130.71, 130.97, 133.10, 165.89, 169.46, 169.66, 170.17, 170.75, 194.12; EI ms: m/z = 551 (M^+); anal. calcd. for $C_{24}H_{25}NO_{10}S_2$ (551.59): C = 52.26, H = 4.57, N = 2.54; found: C = 52.40, H = 4.78, N = 2.35.

*5-((Z)-(4-Methoxybenzylidene)-3-(2′,3′,4′,6′-tetra-O-acetyl-β-D-glucopyranosyl)-2-thioxo-4-thiazolidinone (**11b**).* This compound has mp 231−233 °C; yield 0.44 g (76%); IR, KBr (cm^{-1}): 1752 (CO), 1747 (CO), 1236 (CS); ^{1}H NMR (300 MHz, $CDCl_3$, δ, ppm): 1.94, 2.05, 2.07, 2.10 (12H, 4s, 4Ac), 3.87 (4H, m, OCH_3, 5′-H), 4.18−4.29 2H, (2H, m, 6′-H, 6″-H), 5.29 (1H, dd, J = 9.7, 9.7 Hz, 4′-H), 5.39 (1H, dd, J = 9.3, 9.3 Hz, 2′-H), 6.16 (1H, dd, J = 9.2, 9.2 Hz, 3′-H), 6.35 (1H, d, J = 9.4 Hz, 1′-H), 7.00, 7.44 (4H, 2d, J = 9.5 Hz, 4H, Ar−H), 7.68 (1H, s, =CH); ^{13}C NMR (300 MHz, $CDCl_3$, δ, ppm): 20.42, 20.61, 20.64, 20.78, 55.54, 61.67, 67.74, 73.29, 74.80, 81.76, 114.92, 117.27, 125.78, 132.89, 134.20, 161.84, 166.04, 169.43, 169.58, 170.14, 170.71, 194.11; EI ms: m/z = 581 (M^+); anal. calcd. for $C_{25}H_{27}NO_{11}S_2$ (581.61): C = 51.63, H = 4.68, N = 2.41; found: C = 51.74, H = 4.90, N = 2.36.

*5-((Z)-(2,4-Dichlorobenzylidene)-3-(2′,3′,4′,6′-tetra-O-acetyl-β-D-glucopyranosyl)-2-thioxo-4-thiazolidinone (**11c**).* This compound has mp 230−232 °C; yield 0.54 g (87%); IR, KBr (cm^{-1}): 1754 (CO), 1746 (CO), 1230 (CS); ^{1}H NMR (300 MHz, $CDCl_3$, δ, ppm): 1.92, 2.04, 2.08, 2.12 (12H, 4s, 4Ac), 3.86 (1H, m, 5′-H), 4.17−4.30 (2H, m, 6′-H, 6″-H), 5.28 (1H, dd, J = 9.6, 9.6 Hz, 4′-H), 5.37 (1H, dd, J = 9.4, 9.4 Hz, 2′-H), 6.17 (1H, dd, J = 9.3, 9.2 Hz, 3′-H), 6.36 (1H, d, J = 9.5 Hz, 1′-H), 7.24, 7.60 (3H, m, Ar−H), 7.68 (1H, s, =CH); EI ms: m/z = 620 (M^+); anal. calcd. for $C_{24}H_{23}Cl_2NO_{10}S_2$ (620.48): C = 46.46, H = 3.74, N = 2.26; found: C = 46.61, H = 3.90, N = 2.18.

*5-((Z)-(2-Hydroxy-3-methoxybenzylidene)-3-(2′,3′,4′,6′-tetra-O-acetyl-β-D-glucopyranosyl)-2-thioxo-4-thiazolidinone (**11d**).* This compound was separated as yellow foams; yield 0.52 g (86%); IR, KBr (cm^{-1}): 1752 (CO), 1746 (CO), 1240 (CO); ^{1}H NMR (300 MHz, $CDCl_3$, δ, ppm): 1.96, 2.02, 2.07, 2.18 (12H, 4s, 4Ac), 3.86 (3H, s, OCH_3), 4.12−4.32 (3H, m, 5′-H, 6′-H, 6″-H), 5.26 (1H, dd, J = 9.7, 9.90 Hz, 4′-H), 5.52 (1H, dd, J = 9.5, 9.6 Hz, 2′-H), 6.29 (1H, dd, J = 9.4, 9.6 Hz, 3′-H), 6.33 (1H, d, J = 9.6 Hz, 1′-H), 6.52 (1H, s, OH), 6.90 (3H, m, Ar−H), 8.16 (1H, s, =CH); EI ms: m/z = 597 (M^+); anal. calcd. for $C_{25}H_{27}NO_{12}S_2$ (597.61): C = 50.24, H = 4.55, N = 2.34; found: C = 50.48, H = 4.86, N = 2.21.

*5-((Z)-(3,4-Methylenedioxybenzylidene)-3-(2′,3′,4′,6′-tetra-O-acetyl-β-D-glucopyranosyl)-2-thioxo-4-thiazolidinone (**11e**).* This compound has mp 196−198 °C; yield 0.56 g (94%); (lit.,[65] mp 194−196 °C, yield 78%); IR, KBr (cm^{-1}): 1750 (CO), 1746 (CO), 1226 (CS); ^{1}H NMR (300 MHz, $CDCl_3$, δ, ppm): 1.94, 2.04, 2.07, 2.10 (12H, 4s, 4Ac), 3.88 (1H, m, 5′-H), 4.12−4.25 (2H, m, 6′-H, 6″-H), 5.28 (1H, dd, J = 9.7, 9.7 Hz, 4′-H), 5.39 (1H, dd, J = 9.4, 9.4 Hz, 2′-H), 6.06 (2H, s, OCH_2O), 6.15 (1H, dd, J = 9.2, 9.2 Hz, 3′-H), 6.34 (1H, d, J = 9.4 Hz, 1′-H), 6.89−7.05 (3H, m, Ar−H), 7.60 (1H, s, =CH); ^{13}C NMR (300 MHz, $CDCl_3$, δ, ppm): 20.40, 20.52, 20.60, 20.76, 61.70, 67.81, 73.32, 74.87, 81.82, 102.09, 109.23, 109.36, 118.01, 127.46, 127.61, 134.14, 148.75, 150.24, 165.97, 169.42, 169.59, 170.13, 170.69, 193.87; EI ms: m/z = 595 (M^+); anal. calcd. for $C_{25}H_{25}NO_{12}S_2$ (595.60): C = 50.41; H = 4.23, N = 2.35; found: C = 50.60, H = 4.52, N = 2.24.

*5-((Z)-(3,4-Ethylenedioxybenzylidene)-3-(2′,3′,4′,6′-tetra-O-acetyl-β-D-glucopyranosyl)-2-thioxo-4-thiazolidinone (**11f**).* This compound was separated as yellow foams; yields 0.54 g (88%); IR, KBr (cm^{-1}): 1750 (CO), 1744 (CO), 1232

https://doi.org/10.1021/acsomega.3c00641
ACS Omega 2023, 8, 13300−13314

(CS); ^{1}H NMR (300 MHz, $CDCl_3$, δ, ppm): 1.94, 2.04, 2.06, 2.10 (12H, 4s, 4Ac), 3.87 (1H, m, 5′-H), 4.22−4.33 (6H, m, 6′-H, 6″-H, 2 OCH_2), 5.28 (1H, dd, J = 9.7, 9.7 Hz, 4′-H), 5.38 (1H, dd, J = 9.3, 9.3 Hz, 2′-H), 6.15 (1H, dd, J = 9.2, 9.2 Hz, 3′-H), 6.34 (1H, d, J = 9.4 Hz, 1′-H), 6.92−7.02 (3H, m, Ar−H), 7.60 (1H, s, =CH); ^{13}C NMR (300 MHz, $CDCl_3$, δ, ppm): 20.40, 20.60, 20.63, 20.77, 61.70, 64.14, 64.70, 67.80, 73.36, 74.88, 81.82, 118.13, 118.28, 119.46, 125.21, 126.70, 134.08, 144.04, 146.45, 165.97, 169.40, 169.54, 170.13, 170.69; EI ms: m/z = 609 (M^+); anal. calcd. for $C_{26}H_{27}NO_{12}S_2$ (609.62): C = 51.22, H = 4.46, N = 2.30; found: C = 51.36, H = 4.80, N = 2.12.

General Procedures for the Synthesizing ***12a−f****. Method A.* At 0 °C, protected nucleosides **11a−f** (1 mmol) in 15 mL of anhydrous MeOH were stirred while NaOMe (0.06 g, 1.1 mmol) was gradually added. A further two hours at room temperature was spent stirring the reaction mixture. The resulting solution was then supplemented with an ion-exchange resin (Amberlite IR-120, H+-form), which had previously been washed with MeOH. The mixture was stirred for five minutes, filtered, and vacuum evaporated. The products **12a−f** were obtained as yellow solids after the residue was purified using flash chromatography (eluent: $CHCl_3$/MeOH, eluent: 0−5%).

*5-((Z)-Benzylidene)-3-(β-D-glucopyranosyl)-2-thioxo-4-thiazolidinone (**12a**).* This compound has mp 153−155 °C; yield 352 mg (92%) (lit.,[65] mp 104−110 °C, yield 96%); IR, KBr (cm^{-1}): 3390 (OH), 1717 (CO), 1230 (OH); ^{1}H NMR (300 MHz, DMSO-d_6, δ, ppm): 3.13 (1H, m, 1H, 4′-H), 3.24 (3H, m, 5′-H, 6′-H), 3.72 (1H, m, 1H, 3′-H), 4.40 (1H, m, 2′-H), 4.65 (1H, d, J = 4.6 Hz, 6′−OH), 5.12 (1H, t, J = 5.1 Hz, 4′−OH), 5.23 (1H, d, J = 3.9 Hz, 3′−OH), 5.44 (1H, d, J = 5.0 Hz, 2′−OH), 5.85 (1H, d, J = 9.1 Hz, 1′-H); ^{13}C NMR (300 MHz, DMSO-d_6, δ, ppm): 60.74, 67.45, 69.54, 76.95, 80.35, 84.74, 120.59, 131.10, 125.37, 129.55, 130.49, 132.68, 165.91, 195.36; EI ms: m/z = 383 (M^+); anal. calcd. for $C_{16}H_{17}NO_6S_2$ (383.44): C = 50.12, H = 4.47, N = 3.65, found: C = 50.27, H = 4.58, N = 3.60.

*5-((Z)-(4-Methoxybenzylidene)-3-(β-D-glucopyranosyl)-2-thioxo-4-thiazolidinone (**12b**).* This compound has mp 172−174 °C; yield 359 mg (87%); IR, KBr (cm^{-1}): 3398 (OH), 1712 (CO), 1225 (CS); ^{1}H NMR (300 MHz, DMSO-d_6, δ, ppm): 3.16 (1H, m, 4′-H), 3.20−3.44 (3H, m, 5′-H, 6′-H), 3.70 (1H, m, 3′-H), 3.84 (3H, s, OCH_3), 4.40 (1H, m, 2′-H), 4.64 (1H, t, J = 5.7 Hz, 6′−OH), 5.10 (1H, t, J = 5.3 Hz, 4′−OH), 5.21 (1H, d, J = 4.1 Hz, 3′−OH), 5.42 (1H, t, J = 4.1 Hz, 2′−OH), 5.85 (1H, d, J = 9.3 Hz, 1′-H), 7.14, 7.62 (4H, 2d, J = 8.6 Hz, Ar−H), 7.71 (1H, s, =CH); ^{13}C NMR (300 MHz, DMSO-d_6): 55.52, 60.74, 67.45, 69.52, 77.01, 80.28, 84.68, 117.21, 133.17, 115.17, 125.25, 132.90, 161.55, 166.13, 195.26; EI ms: m/z = 413 (M^+); anal. calcd. for $C_{17}H_{19}NO_7S_2$ (413.47): C = 49.38, H = 4.63, N = 3.39, found: C = 49.60, H = 4.75, N = 3.32.

*5-((Z)-(2,4-Dichlorobenzylidene)-3-(β-D-glucopyranosyl)-2-thioxo-4-thiazolidinone (**12c**).* This compound has mp 186−188 °C; yield 320 mg (71%); IR, KBr (cm^{-1}): 3396 (OH), 1714 (CO), 1230 (CS); ^{1}H NMR (300 MHz, DMSO-d_6, δ, ppm): 3.15 (1H, m, 4′-H), 3.16−3.45 (3H, m, 5′-H, 6′-H), 3.72 (1H, m, 1H, 3′-H), 4.38 (1H, m, 2′-H), 4.66 (1H, t, J = 5.8 Hz, 6′-OH), 5.15 (1H, d, J = 5.5 Hz, 4′-OH), 5.26 (1H, d, J = 4.9 Hz, 3′−OH), 5.47 (1H, t, J = 4.8 Hz, 2′−OH), 5.85 (1H, d, J = 9.4 Hz, 1′-H), 7.58−7.88 (4H, m, Ar−H, = CH); ^{13}C NMR (300 MHz, DMSO-d_6, δ, ppm): 61.00, 67.61, 69.81, 77.22, 80.73, 85.02, 124.93, 125.40, 126.37, 128.54, 129.82, 130.06, 130.57, 135.58, 136.04, 165.46, 194.79; EI ms: m/z = 452 (M^+); anal. calcd. for $C_{16}H_{15}Cl_2NO_6S_2$ (452.33): C = 42.48, H = 3.34, N = 3.10; found: C = 42.66, H = 3.50, N = 3.02.

*5-((Z)-(2-Hydroxy-3-methoxybenzylidene)-3-(β-D-glucopyranosyl)-2-thioxo-4-thiazolidinone (**12d**).* This compound has mp 204−206 °C; yield 352 mg (82%); IR, KBr (cm^{-1}): 3397 (OH), 1718 (CO), 1228 (CS); ^{1}H NMR (300 MHz, DMSO-d_6 + D_2O, δ, ppm): 3.36−3.85 (5H, m, 4′-H, 5′-H, 6′-H, 3′-H), 4.38 (4H, m, 2′-H, OCH_3), 4.70 (1H, t, J = 5.8 Hz, 6′−OH), 5.79 (1H, d, J = 9.0 Hz, 1′-H), 6.95−7.11 (3H, m, Ar−H), 7.94 (1H, s, = CH); ^{13}C NMR ^{1}H NMR (300 MHz, DMSO-d_6 + D_2O, δ, ppm): 55.94, 60.35, 64.93, 68.27, 74.26, 78.92, 85.38, 114.43, 119.52, 119.78, 120.08, 120.50, 128.27, 146.81, 147.99, 165.87, 195.92; EI ms: m/z = 429 (M^+); anal. calcd. for $C_{17}H_{19}NO_8S_2$ (429.46): C = 47.54, H = 4.46, N = 3.26; found: C = 47.78, H = 4.69, N = 3.17.

*5-((Z)-(3,4-Methylenedioxybenzylidene)-3-(β-D-glucopyranosyl)-2-thioxo-4-thiazolidinone (**12e**).* This compound has mp 205−207 °C; yield: 367 mg (86%); IR, KBr (cm^{-1}): 3398 (OH), 1717 (CO), 1225 (CS); ^{1}H NMR ^{1}H NMR (300 MHz, DMSO-d_6 δ, ppm): 3.09 (1H, m, 4′-H), 3.12−3.43 (3H, m, 5′-H, 6′-H), 3.72 (1H, m, 3′-H), 4.39 (1H, ddd, J = 4.6, 8.9, 13.5 Hz, 2′-H), 4.64 (1H, t, J = 4.3 Hz, 6′−OH), 5.11 (1H, d, J = 5.0 Hz, 4′−OH), 5.21 (1H, s, 3′−OH), 5.42 (1H, t, J = 4.9 Hz, 1H, 2′−OH), 5.84 (1H, d, J = 9.4 Hz, 1′-H), 6.15 (2H, s, OCH_2O), 7.06−7.24 (3H, m, Ar−H), 7.67 (1H, s, =CH); ^{13}C NMR (300 MHz, DMSO-d_6 δ, ppm): 61.26, 67.84, 70.11, 77.68, 80.98, 85.18, 102.46, 109.61, 109.83, 118.33, 127.24, 127.35, 133.29, 148.63, 150.16, 166.17, 195.40; EI ms: m/z = 427 (M^+); anal. calcd. for $C_{17}H_{17}NO_8S_2$ (427.45): C = 47.77, H = 4.01, N = 3.28; found: C = 47.89, H = 4.24, N = 3.11.

*5-((Z)-(3,4-Ethylenedioxybenzylidene)-3-(β-D-glucopyranosyl)-2-thioxo-4-thiazolidinone (**12f**).* This compound has mp 198−200 °C; yield: 370 mg (84%); IR, KBr (cm^{-1}): 3396 (OH), 1718 (CO), 1230 (CS); ^{1}H NMR (300 MHz, DMSO-d_6 δ, ppm): 3.14 (1H, m, 1H, 4′-H), 3.17−3.42 (3H, m, 5′-H, 6′-H), 3.69 (1H, m, 1H, 3′-H), 4.32 (4H, d, J = 4.7 Hz, $2CH_2$), 4.39 (1H, ddd, J = 5.0, 8.9, 13.7 Hz, 2′-H), 4.64 (1H, t, J = 5.7 Hz, 6′−OH), 5.10 (1H, d, J = 5.4 Hz, 4′−OH), 5.21 (1H, d, J = 4.6 Hz, 1H, 3′−OH), 5.40 (1H, d, J = 4.8 Hz, 2′−OH), 5.84 (1H, d, J = 9.3 Hz, 1′-H), 7.03−7.17 (3H, m, Ar−H), 7.65 (1H, s, 1H, =CH); ^{13}C NMR (300 MHz, DMSO-d_6 δ, ppm): 61.25, 64.20, 64.79, 67.82, 70.10, 77.67, 80.97, 85.16, 118.34, 118.49, 119.67, 124.72, 126.48, 133.08, 144.10, 146.55, 166.13, 195.42; EI ms: m/z = 441 (M^+); anal. calcd. for $C_{18}H_{19}NO_8S_2$ (441.48): C = 48.97, H = 4.34, N = 3.17; found: C = 49.08, H = 4.50, N = 2.92.

Method B. To a mixture of the protected nucleoside **6** (295 mg, 1 mmol), anhydrous morpholine (0.09 g, 1 mmol) and anhydrous ethanol (10 mL) was added benzaldehyde (0.11 g, 1 mmol). The mixture was stirred until the starting material was consumed (12 h; TLC). The reaction mixture was neutralized with HCl/MeOH. After stirring for 5 min, the solution was evaporated in vacuo and the residue was purified by flash chromatography (eluent 0−5%, $CHCl_3$/MeOH) to afford 345 mg (90%) of **12a** as yellow solid.

7. BIOLOGY

7.1. Cytotoxicity Using MTT Assay. HepG2, MCF-7, and A549 cancer cells, as well as THLE2, MCF-10A, and WISH normal cells, were bought from the National Research Institute

https://doi.org/10.1021/acsomega.3c00641
ACS Omega 2023, 8, 13300−13314

Table 5. Sequences of the forward and reverse primers

Gene	Forward	Reverse
P53	5′-CCCCTCCTGGCCCCTGTCATCTTC-3′	5′-GCAGCGCCTCACAACCTCCGTCAT-3′
Bax	5′-GTTTCATCCAGGATCGAGCAG-3′	5′-CATCTTCTTCCAGATGGTGA-3′
CASP-3	5′-TGGCCCTGAAATACGAAGTC-3′	5′-GGCAGTAGTCGACTCTGAAG-3′
CASP-9	5′-CGAACTAACAGGCAAGCAGC-3′	5′-ACCTCACCAAATCCTCCAGAAC-3′
Bcl-2	5′-CCTGTGGATGACTGAGTACC-3′	5′-GAGACAGCCAGGAGAAATCA-3′
β-actin	5′-GTGACATCCACACCCAGAGG-3′	5′-ACAGGATGTCAAAACTGCCC-3′

of Egypt and cultured in RPMI-1640/DMEM media supplemented with L-glutamine (Lonza Verviers SPRL, Belgium, cat#12−604F). Fetal bovine serum (Sigma-Aldrich, MO, USA) and penicillin−streptomycin at a concentration of 10% and 1%, respectively, were added to both cell lines (Lonza, Belgium). All cells were incubated at 37 °C in 5% carbon dioxide atmosphere (NuAire). In a 96-well plate, cells were seeded at a density of 5,000 cells per well in triplicate. Cells were exposed to compounds at concentrations of 0.01, 0.1, 1, 10, and 100 μM. Doxorubicin was used as positive control. Cell viability was assessed after 48 h using MTT assay (Promega, USA).[66] An ELISA microplate reader was used to measure the absorbance at 690 nm to calculate the viability at each concentration using $(100 - (Abs_{Sample}/Abs_{Control}) \times 100$. IC_{50} values were calculated using GraphPad Prism 7, and viability was evaluated in comparison to a control group, using standard procedures described in the literature.[67]

7.2. Topo II and DNA Intercalation Assay. Topoisomerase II (TopoGEN, Inc., Columbus) and DNA intercalator (methyl green, 20 mg; Sigma-Aldrich) inhibitory activities were measured. Inhibition percentage of compounds was calculated using the following equation: $100 - \left[\left(\frac{Abs_{control}}{Abs_{treated}} - Control\right)\right]$ using the curves of percentage inhibition of five concentrations of each compound; IC_{50} was calculated using GraphPad Prism7 software.[68]

7.3. Investigation of Apoptosis. *7.3.1. Annexin V/PI Staining and Cell Cycle Analysis.* Overnight, $(3-5) \times 10^5$ HepG2 cells were seeded into 6-well culture plates. The cells were subsequently exposed to compound **12f** for 48 h at concentrations of the IC_{50} value. The next step involved collecting medium supernatants and cells and rinsing them with ice-cold PBS. The next step was suspending the cells in 100 μL of annexin binding buffer solution 25 mM $CaCl_2$, 1.4 M NaCl, and 0.1 M Hepes/NaOH, pH 7.4, and incubation with Annexin V-FITC solution (1:100) and propidium iodide (PI) at a concentration equaling 10 μg/mL in the dark for 30 min.[69−71]

7.3.2. Real-Time Polymerase Chain Reaction for the Selected Genes. Apoptosis genes of P53, Bax, Caspases-3,8,9, and Bcl-2 were analyzed for their expression to investigate the apoptotic pathway. HepG2 cells were then treated with compound **12f** at their IC_{50} values for 48 h. After treatment, cells were collected following the treatment period, and the RNeasy Mini Kit was used to extract the total RNA (Qiagen, Hilden, Germany). Then, 500 ng of RNA was used to create cDNA (*i*-Script cDNA synthesis kit, BioRad, Hercules, USA). Finally, 25 μL of Fluocycle II SYBR (Euroclone, Milan, Italy), 10 ng of cDNA, and 2 μL of 10 μM for forward and reverse primers (Table 5.) were used for each RT-PCR reaction. 19 μL of nuclease-free water was added to finish the reaction mixture. RT-PCR reaction was carried out following routine work. The C_t values were then used to determine the relative expression of each gene in each sample after normalization to the actin housekeeping gene.[72−74]

7.3.3. In Silico Studies. Molecular modeling studies were conducted on a Linux computer using Chimera-UCSF and AutoDock Vina. Grid-box dimensions enclosing the cocrystallized ligands, which were earlier created and optimized using Maestro, were used to locate binding sites within the proteins. After standard procedures, the Topo II (PDB = 3QX3) protein structures were docked against the chemicals under investigation using AutoDock Vina.[75−78] The Vina program was used to create optimal and energetically preferable protein and ligand structures. Binding activities and binding energies were used to make sense of the information gleaned through molecular docking. Chimera was then used for the visualization.

■ ASSOCIATED CONTENT

Supporting Information

The Supporting Information is available free of charge at https://pubs.acs.org/doi/10.1021/acsomega.3c00641.

^{1}H NMR, ^{13}C NMR, IR, and MS spectra of the new synthesized compounds (PDF)

■ AUTHOR INFORMATION

Corresponding Author

Ahmed I. Khodair − *Chemistry Department, Faculty of Science, Kafrelsheikh University, 33516 Kafrelsheikh, Egypt;* orcid.org/0000-0001-6674-4561; Email: khodair2020@yahoo.com

Authors

Fatimah M. Alzahrani − *Department of Chemistry, College of Science, Princess Nourah bint Abdulrahman University, Riyadh 11671, Saudi Arabia*

Mohamed K. Awad − *Theoretical Applied Chemistry Unit (TACU), Chemistry Department, Faculty of Science, Tanta University, 6632110 Tanta, Egypt*

Siham A. Al-Issa − *Department of Chemistry, College of Science, Princess Nourah bint Abdulrahman University, Riyadh 11671, Saudi Arabia*

Ghaferah H. Al-Hazmi − *Department of Chemistry, College of Science, Princess Nourah bint Abdulrahman University, Riyadh 11671, Saudi Arabia*

Mohamed S. Nafie − *Chemistry Department (Biochemistry program), Faculty of Science, Suez Canal University, 41522 Ismailia, Egypt;* orcid.org/0000-0003-4454-6390

Complete contact information is available at: https://pubs.acs.org/10.1021/acsomega.3c00641

Notes

The authors declare no competing financial interest.

https://doi.org/10.1021/acsomega.3c00641
ACS Omega 2023, 8, 13300−13314

■ ACKNOWLEDGMENTS

This research was funded by the Deanship of Scientific Research at Princess Nourah bint Abdulrahman University, through the Research Funding Program (FRP-43-4).

■ REFERENCES

(1) Moellering, R. C., Jr. Current treatment options for community-acquired methicillin-resistant staphylococcus aureus infection. *Clin. Infect. Dis.* **2008**, *46*, 1032−1037.
(2) Liu, J. C.; Zheng, C. J.; Wang, M. X.; Li, Y. R.; Ma, L. X.; Hou, S. P.; Piao, H. R. Synthesis and evaluation of the antimicrobial activities of 3-((5-phenyl-1,3,4-oxadiazol-2-yl)methyl)-2-thioxothiazolidin-4-one derivatives. *Eur. J. Med. Chem.* **2014**, *74*, 405−410.
(3) Cutshall, N. S.; O'Day, C.; Prezhdo, M. Rhodanine derivatives as inhibitors of jsp-1. *Bioorg. Med. Chem. Lett.* **2005**, *15*, 3374−3379.
(4) Alegaon, S. G.; Alagawadi, K. R.; Sonkusare, P. V.; Chaudhary, S. M.; Dadwe, D. H.; Shah, A. S. Novel Imidazo[2,1-b][1,3,4]thiadiazole Carrying Rhodanine-3-acetic Acid as Potential Antitubercular Agents. *Bioorg. Med. Chem. Lett.* **2012**, *22*, 1917−1921.
(5) Rajamaki, S.; Innitzer, A.; Falciani, C.; Tintori, C.; Christ, F.; Witvrouw, M.; Debyser, Z.; Massa, S.; Botta, M. Exploration of novel thiobarbituric acid-, rhodanine-and thiohydantoin-based hiv-1 integrase inhibitors. *Bioorg. Med. Chem. Lett.* **2009**, *19*, 3615−3618.
(6) Kumar, G.; Parasuraman, P.; Sharma, S. K.; Banerjee, T.; Karmodiya, K.; Surolia, N.; Surolia, A. Discovery of a rhodanine class of compounds as inhibitors of plasmodium falciparum enoyl-acyl carrier protein reductase. *J. Med. Chem.* **2007**, *50*, 2665−2675.
(7) Ergenç, N.; Çapan, G.; Günay, N. S.; Özkirimli, S.; Güngör, M.; Özbey, S.; Kendi, E. Synthesis and hypnotic activity of new 4-thiazolidinone and 2-thioxo-4,5-imidazolidinedione derivatives. *Archiv der Pharmazie (Weinheim)* **1999**, *332*, 343−347.
(8) Rauter, A. P.; Padilha, M.; Figueiredo, J. A.; Ismael, M. I.; Justino, J.; Ferreira, H.; Ferreira, M. J.; Rajendran, C.; Wilkins, R.; Vaz, P. D.; Calhorda, M. J. Bioactive pseudo-c-nucleosides containing thiazole, thiazolidinone, and tetrazole rings. *J. Carbohydr. Chem.* **2005**, *24*, 275−296.
(9) Tomasic, T.; Masic, L. P. Rhodanine as a privileged scaffold in drug discovery. *Curr. Med. Chem.* **2009**, *16*, 1596−1629.
(10) Tomasic, T.; Masic, L. P. Rhodanine as a scaffold in drug discovery: a critical review of its biological activities and mechanisms of target modulation. *Expert opin. drug discov.* **2012**, *7*, 549−560.
(11) Hirsova, P.; Dolezel, J.; Kucerova-Chlupacova, M.; Kunes, J.; Pilarova, V.; Novakova, L.; Opletalova, V. (*Z*)-3-Amino-5-(pyridin-2-ylmethylidene)-2-thioxo-1,3thiazolidin-4-one. *Molbank* **2015**, *2015*, M872.
(12) Dolezel, J.; Opletalova, V.; Vejsova, M.; Hirsova, P. Evaluation of thiazolidine derivatives. *Acta Pharm. Sci.* **2007**, *49*, 31−43.
(13) Petrik, P.; Kunes, J.; Vejsova, M.; Jampilek, J.; Spaningerova, E.; Kesetovicova, D.; Vlckova, M.; Majd, M.; Kalafutova, S.; Opletalova, V. Antifungal and antimycobacterial properties of 5-arylmethylidenerhodanines and their N_3-substituted analogues. *Acta Pharm. Sci.* **2007**, *49*, 77−87.
(14) Dolezel, J.; Hirsova, P.; Opletalova, V.; Dohnal, J.; Vejsova, M.; Kunes, J.; Jampilek, J. Rhodanineacetic acid derivatives as potential drugs: preparation, hydrophobic properties and antifungal activity of (5-arylalkylidene-4-oxo-2-thioxo-1,3-thiazolidin-3-yl)acetic acids. *Molecules.* **2009**, *14*, 4197−4212.
(15) Opletalova, V.; Dolezel, J.; Buchta, V.; Vejsova, M.; Paterova, P. Antifungal effects of (5Z)-5-arylmethylidenerhodanines with a special view to members of mucorales. *Folia Pharm. Univ. Carol.* **2014**, *42*, 7−13.
(16) Khodair, A. I. Convenient synthesis of 2-arylidene-5H-thiazolo[2,3-b]quinazoline-3,5[2H]-diones and their benzoquinazoline derivatives. *J. Heterocycl. Chem.* **2002**, *39*, 1153−1160.
(17) Khodair, A. I.; Gesson, J.-P A new approach for the *N*- and *S*-galactosylation of 5-arylidene-2-thioxo-4-thiazolidinones. *Carbohydr. Res.* **2011**, *346*, 2831−2337.
(18) Khodair, A. I.; Awad, M. K.; Gesson, J.-P.; Elshaier, Y. A. M. M New N-ribosides and N-mannosides of rhodanine derivatives with anticancer activity on leukemia cell line: Design, synthesis, DFT and molecular modelling studies. *Carbohyd. Res.* **2020**, *487*, 107894.
(19) Opletalova, V.; Dolezel, J.; Kralova, K.; Pesko, M.; Kunes, J.; Jampilek, J. Synthesis and characterization of (*Z*)-5-arylmethylidenerhodanines with photosynthesis-inhibiting properties. *Molecules* **2011**, *16*, 5207−5227.
(20) Ohishi, Y.; Mukai, T.; Nagahara, M.; Yajima, M.; Kajikawa, N.; Miyahara, K.; Takano, T. Preparations of 5-alkylmethylidene-3-carboxymethylrhodanine derivatives and their aldose reductase inhibitory activity. *Chem. Pharm. Bull.* **1990**, *38*, 1911−1919.
(21) Momose, Y.; Meguro, K.; Ikeda, H.; Hatanaka, C.; Oi, S.; Sohda, T. Studies on antidiabetic agents X: synthesis and biological activities of pioglitazone and related compounds. *Chem. Pharm. Bull.* **1991**, *39*, 1440−1445.
(22) Sudo, K.; Matsumoto, Y.; Matsushima, M.; Fujiwara, M.; Konno, K.; Shimotohno, K.; Shigeta, S.; Yokota, T. Novel hepatitis C virus protease inhibitors: thiazolidine derivative. *Biochem. Biophys. Res. Commun.* **1997**, *238*, 643−647.
(23) Sim, M. M.; Ng, S. B.; Buss, A. D.; Crasta, S. C.; Goh, K. L.; Lee, S. K. Rhodanines as novel inhibitors of UDP-N-acetylmuramate/L-alanine ligase. *Bioorg. Med. Chem. Lett.* **2002**, *12*, 697−699.
(24) Frlan, R.; Kovac, A.; Blanot, D.; Gobec, S.; Pecar, S.; Obreza, A. Design and synthesis of novel *N*-benzylidenesulfonohydrazide inhibitors of MurC and MurD as potential antibacterial agents. *Molecules* **2008**, *13*, 11−30.
(25) Kristan, K.; Kotnik, M.; Oblak, M.; Urleb, U. J. New high-throughput fluorimetric assay for discovering inhibitors of UDP-N-acetylmuramyl-L-alanine: D-glutamate (MurD) ligase. *Biomol. Screen.* **2009**, *14*, 412−418.
(26) Schemmel, K. E.; Padiyara, R. S.; D'Souza, J. J. Aldose reductase inhibitors in the treatment of diabetic peripheral neuropathy: A review. *J. Diabetes Complicat.* **2010**, *24*, 354−360.
(27) Bulic, B.; Pickhardt, M.; Khilstunova, I.; Biernat, J.; Mandelkow, E. M.; Mandelkow, E.; Waldmann, H. Rhodanine-based tau aggregation inhibitors in cell models of tauopathy. *Angew. Chem., Int. Ed.* **2007**, *46*, 9215−9219.
(28) Zeiger, E.; Anderson, B.; Haworth, S.; Lawlor, T.; Mortelmans, W. Salmonella mutagenicity tests: III. Results from the testing of 255 chemicals. *Environ. Mutagen.* **1987**, *9*, 1−60.
(29) Hotta, N.; Akanuma, Y.; Kawamori, R.; Matsuoka, K.; Oka, Y.; Shichiri, M.; Toyota, T.; Nakashima, M.; Yoshimura, I.; Sakamoto, N.; Shigeta, Y. Long-term clinical effects of epalrestat, an aldose reductase inhibitor, on diabetic peripheral neuropathy: the 3-year, multicenter, comparative aldose reductase inhibitor-diabetes complications trial. *Diabetes Care.* **2006**, *29*, 1538−1544.
(30) Moorthy, B. T.; Ravi, S.; Srivastava, M.; Chiruvella, K. K.; Hemlal, H.; Joy, O.; Raghavan, S. C. Novel rhodanine derivatives induce growth inhibition followed by apoptosis. *Med. Chem. Lett.* **2010**, *20*, 6297−6301.
(31) Azizmohammadi, M.; Khoobi, M.; Ramazani, A.; Emami, S. 2*H*-Chromene derivatives bearing thiazolidine-2,4-dione, rhodanine or hydantoin moieties as potential anticancer agents. *Eur. J. Med. Chem.* **2013**, *59*, 15−22.
(32) Mandal, S. P.; Mithuna, M.; Garg, A.; Sahetya, S. S.; Nagendra, S. R.; Sripad, H. S.; Manjunath, M. M.; Sitaram, S.; Soni, M.; Baig, R. N.; Kumar, S. V.; Kumar, B. R. P. Novel rhodanines with anticancer activity: design, synthesis and CoMSIA study. *RSC Adv.* **2016**, *6*, 58641−58653.
(33) Kumar, R.; Lown, J. W. Synthesis and antitumor cytotoxicity evaluation of novel thiazole-containing glycosylated polyamides. *Eur. J. Org. Chem.* **2003**, *2003*, 4842−4851.
(34) Knight, S. D.; Adams, N. D.; Burgess, J. L.; Chaudhari, A. M.; Darcy, M. G.; Donatelli, C. A.; Luengo, J. I.; Newlander, K. A.; Parrish, C. A.; Ridgers, L. H.; Sarpong, M. A.; Schmidt, S. J.; Van Aller, G. S.; Carson, J. D.; Diamond, M.; Elkins, A. P. A.; Gardiner, C. M.; Garver, E.; Gilbert, S. A.; Gontarek, R. R.; Jackson, J. R.; Kershner, K. L.; Luo, K. L. L.; Raha, K.; Sherk, C. S.; Sung, C. M.;

https://doi.org/10.1021/acsomega.3c00641
ACS Omega 2023, 8, 13300−13314

Sutton, D.; Tummino, P. J.; Grzyn, K. R. W.; Auger, R. J.; Dhanak, D. Discovery of GSK2126458, a higly potent inhibitor of PI3K and the mammalian target of rapamycin. *ACS Med. Chem. Lett.* **2010**, *1*, 39−43.
(35) El-Barbary, A. A.; Khodair, A. I.; Pedersen, E. B.; Nielsen, C. *S*-glucosylated hydantoins as new antiviral agents. *J. Med. Chem.* **1994**, *37*, 73−77.
(36) Al-Obaid, A. M.; EL-Subagh, H. I.; Khodair, A. I.; Elmazar, M. M. A. 5-Substituted 2-thiohydantoin analogs as a novel class of antitumor agents. *Anticancer Drugs* **1996**, *7*, 873−880.
(37) Khodair, A. I. glycosylation of 2-thiohydantoin derivatives. synthesis of some novel *S*-alkylated and *S*-glucosylatedhydantoins. *Carbohydr. Res.* **2001**, *331*, 445−453.
(38) Khodair, A. I. Synthesis of 2-thiohydantoins and their *S*-glucosylated derivatives as potential antiviral and antitumor agents. *Nucleosides, Nucleotides and Nucleic Acids* **2001**, *20*, 1735−1750.
(39) El-Barbary, A. A.; Khodair, A. I.; Pedersen, E. B. Synthesis and antiviral evaluation of hydantoin analogues of azt. *Archiv der Pharmaze (Weinheim)* **1994**, *327*, 653−655.
(40) Khodair, A. I.; Attia, A. M.; Gendy, E. A.; Elshaier, Y. A. M. M.; El-Magd, M. A. Design, synthesis and cytotoxicity evaluation of some novel of *S*-glycoside of 2-thioxopyridine and *N*-glycoside of 2-oxopyridine derivatives as antibreast cancer. *J. Heterocycl. Chem.* **2019**, *56*, 1733−1747.
(41) Khodair, A. I.; Alsafi, M. A.; Nafie, M. S. Synthesis, molecular modeling and anti-cancer evaluation of a series of quinazoline derivatives. *Carbohydr. Res.* **2019**, *486*, 107832.
(42) Khodair, A. I.; Elsafi, M. A.; Al-Essa, S. A. Simple and efficient synthesis of novel 3-substituded-2-thioxo-2,3-dihydro-1*H*-benzo[g]-quinazolin-4-ones and their reactions with alkyl halides and α-glycopyranosyl bromides. *J. Heterocycl. Chem.* **2019**, *56* (9), 2358−2368.
(43) Attia, A. M.; Khodair, A. I.; Gendy, E. A.; El-Magd, M. A.; Elshaier, Y. A. M. M. New 2-oxopyridine/2-thiopyridine derivatives tethered to a benzotriazole with cytotoxicity on MCF7 cell lines and with antiviral activities. *Lett. Drug Des. Discovery* **2020**, *17*, 124−137.
(44) Khodair, A. I.; El-Barbary, A. A.; Imam, D. R.; Kheder, N. A.; Elmalki, F.; Ben Hadda, T. Synthesis, DFT, antiviral, and molecular docking studies of some novel 1,2,4-triazine nucleosides as potential bioactive compounds. *Carbohydr. Res.* **2021**, *500*, 108246.
(45) Khodair, A. I.; Bakare, S. B.; Awad, M. K.; Al-Issa, S. A.; Nafie, M. S. Design, synthesis and computational explorations of novel 2-thiohydantoin nucleosides with cytotoxic activities. *J. Heterocycl. Chem.* **2022**, *59* (4), 664−685.
(46) El-Barbary, A. A.; Imam, D. R.; El-Tahawy, M. M. T.; El-Hallouty, S. M.; Kheder, N. A.; Khodair, A. I. Unexpected synthesis, characterization and comutaional details of novel triazine-pyrrole hybrid nucleosides. *J. Mol. Struct.* **2023**, *1272*, 134182.
(47) Houk, K. N.; Liu, F. Holy grails for computational organic chemistry and biochemistry. *Acc. Chem. Res.* **2017**, *50*, 539−543.
(48) Kabanda, M. M.; Murulana, L. C.; Ozcan, M.; Karadag, F. Quantum chemical studies on the corrosion inhibition of mild steel by some triazoles and benzimidazole derivatives in acidic medium. *Int. J. Electrochem. Sci.* **2012**, *7*, 5035−5056.
(49) Udhayakala, P.; Jayanthi, A.; Rajendiran, T. V. Adsorption and quantum chemical studies on the inhibition potentials of some formazan derivatives. *Der Pharma Chem.* **2011**, *3*, 528−539.
(50) Awad, M. K.; Masoud, M. S.; Shaker, M. A.; Ali, A. E. MP2 and DFT theoretical studies of the geometry, vibrational and electronic absorption spectra of 2-aminopyrimidine. *Res. Chem. Intermed.* **2013**, *39*, 2741−2761.
(51) Atlam, F. M.; Awad, M. K.; El-bastawissy, E. A. Computational simulation of the effect of quantum chemical parameters on the molecular docking of HMG-CoA reductase drugs. *J. Mol. Struct.* **2014**, *1075*, 311−326.
(52) Khodair, A. I.; Bakare, S. B.; Awad, M. K.; Nafie, M. S. Design, synthesis, DFT, molecular modelling studies and biological evaluation of novel 3-substituted (E)-5-(arylidene)-1-methyl-2-thioxoimidazolidin-4-ones with potent cytotoxic activities against breast MCF-7, liver HepG2, and lung A549. *J. Mol. Struct.* **2021**, *1229*, 129805.
(53) Elbadawi, M. M.; Khodair, A. I.; Awad, M. K.; Kassab, S. E.; Elsaady, M. T.; Abdellatif, K. R. A. Design, synthesis and biological evaluation of novel thiohydantoin derivatives as antiproliferative agents: A combined experimental and theoretical assessments. *J. Mol. Struct.* **2022**, *1249*, 131574.
(54) Awad, M. K.; Abdel-Aal, M. F.; Atlam, F. M.; Hekal, H. A. Molecular docking, molecular modeling, vibrational and biological studies of some new heterocyclic α-aminophosphonates. *Spectrochim, Acta Part A: Mol. Biomol. Spect.* **2019**, *206*, 78−88.
(55) El-Borai, M. A.; Awad, M. K.; Rizk, H.F.; Atlam, F. M. Design, Synthesis and Docking study of Novel Imidazolyl Pyrazolopyridine Derivatives as Antitumor Agents Targeting MCF7 Cell Line. *Curr. Org. Chem.* **2018**, *15*, 275−285.
(56) Werbel, L. M.; Headen, N.; Elslager, E. F. 3-Phenylrhodanines as potential antimalarial agents. *J. Med. Chem.* **1968**, *11*, 364−365.
(57) Brown, F. C.; Bradsher, C. K.; Bond, S. M.; Grantham, R. J. Mildew-Preventing Activity of Rhodanine Derivatives. *Ind. Eng. Chem.* **1954**, *46*, 1508−1512.
(58) Khodair, A. I.; Alzahrani, F. M.; Awad, M. K.; Al-Issa, S. A.; Al-Hazmi, G. H.; Nafie, M. S. Design, synthesis, molecular modelling and antitumor evaluation of *S*-glucosylated rhodanines through topo II inhibition and DNA intercalation. *J. Enz. Inhib. and Med. Chem.* **2023**, *38* (1), 2163996.
(59) Walter, W.; Randau, G. Über die Oxydationsprodukte von Thiocarbonsäureamiden, VIII Oxydationsreaktionen an *N*-Acyl-thioamiden. *Justus Liebigs Ann. Chem.* **1965**, *681*, 55−63.
(60) Villemin, D.; Alloum, A. B. Potassium fluoride on alumina: condensation of 3-methyl-2-thiono-4-thiazolidinone with aldehydes synthesis of α-thioacrylic acids and phosphonothionothiazolidinones. *Phosphorus Sulfur Silicon Relat. Elem.* **1993**, *79*, 33.
(61) Ishida, T.; In, Y.; Inoue, M.; Ueno, Y.; Tanaka, C. Structural elucidation of epalrestat (ONO-2235), a potent aldose reductase inhibitor, and isomerization of its double bonds. *Tetrahedron Lett.* **1989**, *30*, 959−962.
(62) Becke, A. D. Density-functional thermochemistry II: the effect of the Perdew-Wang generalized-gradient correlation correction. *J. Chem. Phys.* **1992**, *97*, 9173−9177.
(63) Becke, A. D. A new mixing of Hartree−Fock and local density-functional theories. *J. Chem. Phys.* **1993**, *98*, 1372−1377.
(64) Lee, C.; Yang, W.; Parr, R. G. Development of the colle-salvetti correlation-energy formula into a functional of the electron density. *Phys. Rev. B* **1988**, *37*, 785−789.
(65) Foye, W. O.; Tovivich, P. *N*-glucopyranosyl-5-aralkylidenerhodanines: Synthesis and antibacterial and antiviral activities. *J. Pharm. Sci.* **1977**, *66*, 1607−1611.
(66) Mosmann, T. Rapid colorimetric assay for cellular growth and survival: Application to proliferation and cytotoxicity assays. *J. Immunol. Methods* **1983**, *65*, 55−63.
(67) Tantawy, E. S.; Amer, A. M.; Mohamed, E. K.; Abd Alla, M. M.; Nafie, M. S. Synthesis, characterization of some pyrazine derivatives as anti-cancer agents: In vitro and in Silico approaches. *J. Mol. Struct.* **2020**, *1210*, 128013.
(68) Nafie, M. S.; Amer, A. M.; Mohamed, A. K.; Tantawy, E. S. Discovery of novel pyrazolo[3,4-b]pyridine scaffold-based derivatives as potential PIM-1 kinase inhibitors in breast cancer MCF-7 cells. *Bioorg. Med. Chem.* **2020**, *28*, 115828.
(69) Khalifa, M. M.; Al-Karmalawy, A. A.; Elkaeed, E. B.; Nafie, M. S.; Tantawy, M. A.; Eissa, I. H.; Mahdy, H. A. Topo II inhibition and DNA intercalation by new phthalazine-based derivatives as potent anticancer agents: design, synthesis, anti-proliferative, docking, and in vivo studies. *J. Enzyme Inhib. Med. Chem.* **2022**, *37*, 299−314.
(70) Boraei, A. T. A.; Eltamany, E. H.; Ali, I. A. I.; Gebriel, S. M.; Nafie, M. S. Synthesis of new substituted pyridine derivatives as potent anti-liver cancer agents through apoptosis induction: In vitro, in vivo, and in silico integrated approaches. *Bioor. Chem.* **2021**, *111*, 104877.

https://doi.org/10.1021/acsomega.3c00641
ACS Omega 2023, 8, 13300−13314

(71) Dawood, K. M.; Raslan, M. A.; Abbas, A. A.; Mohamed, B. E.; Abdellattif, M. H.; Nafie, M. S.; Hassan, M. K. Novel bis-thiazole derivatives: synthesis and potential cytotoxic activity through apoptosis with molecular docking approaches. *Front. Chem.* **2021**, *9*, 694870.
(72) Gad, E. M.; Nafie, M. S.; Eltamany, E. H.; Hammad, M. S. A. G.; Barakat, A.; Boraei, A. T. A. Discovery of new apoptosis-inducing agents for breast cancer based on ethyl 2-amino-4,5,6,7-tetra hydrobenzo[b]thiophene-3-carboxylate: synthesis, in vitro, and in vivo activity evaluation. *Molecules* **2020**, *25*, 2523.
(73) Tantawy, M. A.; Shaheen, S.; Kattan, S. W.; Alelwani, W.; Barnawi, I. O.; Elmgeed, G. A.; Nafie, M. S. Cytotoxicity, in silico predictions and molecular studies for androstane heterocycle compounds revealed potential antitumor agent against lung cancer cells. *J. Biomol. Struct. Dyn.* **2022**, *40*, 4352.
(74) ElZahabi, H. S.A.; Nafie, M. S.; Osman, D.; Elghazawy, N. H.; Soliman, D. H.; EL-Helby, A. A. H.; Arafa, R. K. Design, synthesis and evaluation of new quinazolin-4-one derivatives as apoptotic enhancers and autophagy inhibitors with potent antitumor activity. *Eur. J. Med. Chem.* **2021**, *222*, 113609.
(75) Eltamany, E. E.; Elhady, S. S.; Ahmed, H. A.; Badr, J. M.; Noor, A. O.; Ahmed, S. A.; Nafie, M. S. Chemical Profiling, Antioxidant, Cytotoxic Activities and Molecular Docking Simulation of Carrichtera annua DC. (Cruciferae). *Antioxidants.* **2020**, *9*, 1286.
(76) Kishk, S. M.; Kishk, R. M.; Yassen, A. S. A.; Nafie, M. S.; Nemr, N. A.; ElMasry, G.; Al-Rejaie, S.; Simons, C. Molecular Insights into Human Transmembrane Protease Serine-2 (TMPS2) Inhibitors against SARS-CoV2: Homology Modelling, Molecular Dynamics, and Docking Studies. *Molecules* **2020**, *25*, 5007.
(77) Nafie, M. S.; Boraei, A. T. A. Exploration of novel VEGFR2 tyrosine kinase inhibitors via design and synthesis of new alkylated indolyl-triazole Schiff bases for targeting breast cancer. *Bioorg. Chem.* **2022**, *122*, 105708.
(78) Nafie, M. S.; Tantawy, M. A.; Elmgeed, G. A. Screening of different drug design tools to predict the mode of action of steroidal derivatives as anti-cancer agents. *Steroids* **2019**, *152*, 108485.

https://doi.org/10.1021/acsomega.3c00641
ACS Omega 2023, 8, 13300−13314